RESEARCH ARTICLE

ESPL WILEY

Assessing land use effects on ecohydrological partitioning in the critical zone through isotope-aided modelling

Jessica Landgraf[1,2] | Dörthe Tetzlaff[1,2] | Christian Birkel[3,4,5] |
Jamie Lee Stevenson[5] | Chris Soulsby[5]

[1]Department of Ecohydrology and Bigeochemistry, Leibniz Institute of Freshwater Ecology and Inland Fisheries, Berlin, Germany

[2]Department of Geography, Humboldt Universität zu Berlin, Berlin, Germany

[3]Department of Geography – Water and Global Change Observatory, University of Costa Rica, San Jose, Costa Rica

[4]Water Security and Soil Unit, CATIE, Turrialba, Costa Rica

[5]Northern Rivers Institute, School of Geosciences, University of Aberdeen, Aberdeen, Scotland

Correspondence
Jessica Landgraf, Department of Ecohydrology and Bigeochemistry, Leibniz Institute of Freshwater Ecology and Inland Fisheries, Berlin, Germany.
Email: jessica.landgraf@igb-berlin.de

Abstract

Stable water isotopes are naturally occurring conservative tracers that can 'finger-print' water sources and track ecohydrological fluxes across the critical zone (CZ). Parsimonious, tracer-aided models allow effective quantification of the eco-hydrological partitioning of rainfall into different water fluxes. We incorporated stable water isotopes into a one-dimensional, tracer-aided model (EcoIsoPlot) to follow the pathway of precipitation through the CZ at a lowland catchment—the long-term experimental Demnitzer Millcreek Catchment (DMC), Germany—with contrasting vegetation covers (forest, agroforestry, grassland and arable). Precipitation (amount and δ^2H), potential evapotranspiration (PET), leaf area index (LAI), air temperature and relative humidity were used as input data for modelling the growing season of 2021. The year had relatively average overall wetness, but a dry, cold spring with snowfall, and an exceptionally large summer storm event ($\sim$60 mm precipitation). Multi-criteria calibration of the model was conducted using depth-specific soil moisture and soil water δ^2H measurements as targets. The novel incorporation of isotopes into model calibration constrained process representation of the estimated water balance with reasonable simulations and uncertainty bounds for water partitioning. Throughout the soil profile, soil moisture dynamics and stable water isotope variations were captured reasonably well. Green water fluxes (evapotranspiration) were highest at the forest site and blue water fluxes (groundwater recharge) highest at the grassland. Comparing simulations with estimated potential evapotranspiration (ET) and measured groundwater table fluctuations added further confidence to the modelling result. Overall, these may suggest a slight underestimation of ET and slight overestimation of recharge, though the results are similar to previous findings. Our study demonstrated the potential of stable water isotope data to enhance relatively simple, transferrable approaches to ecohydrological modelling of water fluxes in the CZ and to help improve model consistency. Such low-parameterised tracer-aided models have major potential for evidence-based applications to aid management and help stakeholder communication.

KEYWORDS
blue and green water fluxes, critical zone processes, land use effects, stable water isotopes, tracer-aided modelling

1 | INTRODUCTION

Incoming precipitation can be partitioned through a variety of eco-hydrological processes when moving through the critical zone (CZ), which extends from the vegetation canopy to groundwater (Grant & Dietrich, 2017). Understanding and quantifying these processes that partition water into blue (i.e. groundwater recharge and stream flow generation) and green (i.e. evaporation and transpiration) fluxes (Falkenmark & Rockström, 2006) is important to understanding landscape functionality and developing sustainable water management strategies. The main driver of water partitioning in the CZ in many areas is evapotranspiration (ET) (Kool et al., 2014), with transpiration comprising up to 60% of ET at the global scale (Coenders-Gerrits et al., 2014; Schlesinger & Jasechko, 2014). Transpiration is strongly dependent on vegetation cover (Schlesinger & Jasechko, 2014), which further influences processes like interception (Gerrits et al., 2010), infiltration (Zhang et al., 2013), soil water retention (Balist et al., 2022), solar reflection and aerodynamic roughness (Roberts, 2009).

Changing economic priorities, for example, for different food or fibre production, can change vegetation cover and often result in changes in water 'consumption' according to land use (Foley et al., 2005). Hence, sustainable water and land management policies to improve resilience strategies against climate extremes such as droughts (Orth & Destouni, 2018; Tague et al., 2019) as well as climate change-induced shifts in precipitation amounts and patterns (Wunsch et al., 2022) are increasingly the main goals of ecohydrological studies. Understanding vegetation cover effects on water partitioning may help to identify more sustainable alternative land uses, like agroforestry, which may reduce water consumption whilst remaining economically viable (Noordwijk, 2020; Rijal, 2019).

Differentiating water partitioning of ET into evaporation and transpiration is challenging because of multiple, interacting, uncertainties over controls like atmospheric demand, leaf area index (LAI), rooting zone distributions and stomatal resistance (Dubbert & Werner, 2019; Kool et al., 2014). Previous studies have utilised stable water isotopes to help partition water fluxes into evaporation and transpiration using evaporative fractionation signals (Kool et al., 2014; Rothfuss et al., 2010; Sprenger et al., 2016). Further, ecohydrological modelling can conceptualise and quantify the coupled dynamics of water, vegetation, and nutrients and hence support decisions on sustainability of natural resources (Fatichi et al., 2016; Porporato et al., 2015). Specifically, tracer-aided models with isotope tracking can allow water sources and fluxes to be better constrained (Rothfuss et al., 2010) and may help validate physical-based models for water partitioning (Kuppel et al., 2018). Incorporating vegetation dynamics into such models can better quantify ET (Shao et al., 2019) and separate evaporation from transpiration (Kool et al., 2014; Sprenger et al., 2016). For example, a recent study of reforestation by Neill et al. (2021) using the tracer-aided, process-based, EcH$_2$O-iso model found that older, early-stage thicket forest was likely to increase transpiration and interception evaporation compared to non-forested moorland, leading to decreased soil evaporation, groundwater recharge and streamflow in the Scottish Highlands. Another study by Sprenger et al. (2022), incorporating plant water isotopes into StorAge Selection functions (SAS), found winter precipitation to be the main source of ET at the Can Vila catchment in the Spanish Pyrenees mountains. Moreover,

Knighton et al. (2017) found that the incorporation of a plant growth model for ET partitioning substantially improved stream water isotope simulations in spring in a small watershed in the USA.

Here, we investigated water partitioning in the CZ under various land use types in the long-term experimental catchment Demnitzer Mill Creek (DMC), Germany, during the growing season of 2021. The mixed-land use catchment is typical for the drought sensitive lowlands of north-eastern Germany in terms of its landforms, geology, topography, and soils, with forest, grassland, crops and recently developed agroforestry (an increasingly popular agent of land use change). Previous work at the DMC identified the crucial role of land use cover on water partitioning in the local effects of the 2018 European drought. Forests used more water in ET, as well as sourcing transpiration by deeper root uptake of older soil water, whereas grassland root-uptake used shallower soil water with similar ages to soil evaporation (Smith, Tetzlaff, Kleine, et al., 2020). Forests were also shown to be subject to greater moisture stress (because of higher ET), though with more rapid recovery from drought and greater flexibility in root-water uptake compared to grassland (Kleine, Tetzlaff, Smith, Dubbert, & Soulsby, 2021). In contrast, the grassland showed higher and older soil water storage and slower replenishment of deeper soil water (Kleine, Tetzlaff, Smith, Dubbert, & Soulsby, 2021).

Both studies used the model EcH$_2$O-iso, a physically based model combining water and energy fluxes with vegetation carbon allocation. However, as a process-based model, EcH$_2$O-iso requires a variety of substantial input data, is highly parameterised and requires extensive calibration (with the risk of overfitting). The high data needs and computational demands of such models limit transferability to various data-poor ecohydrological settings where the impacts of land use change on water use need to be assessed. As an alternative approach, simpler conceptual, lumped tracer-aided modelling tools require less extensive input data and are potentially more transferable, whilst enabling similar quantification of ecohydrological fluxes and resolving of ET into its component fluxes (Stevenson et al., 2023).

Our study utilised data of precipitation amount and isotopic composition, soil water storage and isotopes monitored in the DMC lowland catchment in 2021, to estimate water fluxes and ecohydrological partitioning under various vegetation covers. This was partly motivated by the increasing need to quantify the water "footprint" of alternative land uses following the 2018 drought which resulted in substantially reduced crop yields in some areas and increased forest tree mortality (Hänsel et al., 2022; Kleine, Tetzlaff, Smith, Dubbert, & Soulsby, 2021; Moravec et al., 2021). We used the lumped, low-parameter, EcoHydroPlot model, which is easy to parameterise for different vegetation cover types (Stevenson et al., 2023), added isotope tracer simulations, and applied it for plot-scale simulations of four different dominant land use and soil units at the DMC catchment. Such a simple, one-dimensional, plot-scale model with a parsimonious concept also has high potential to be used in communicating to stakeholders to underpin management decisions as model concepts are easy to follow. We aimed to quantify water partitioning in the CZ under alternative land uses through the following research questions:

1. How well can a simple, conceptual tracer-aided ecohydrological model capture land use influences on water partitioning in a drought-sensitive catchment?

2. How well can the key ecohydrological interactions that control important CZ processes such as ET and groundwater recharge be quantified and represented?

3. What are the advantages and limitations of using isotopes in such models and how might they be improved?

2 | STUDY AREA

2.1 | Demnitzer Millcreek catchment

The study was conducted in the DMC which is located approximately 60 km east of Berlin (52°23' N, 14°15' E), NE Germany. The catchment is 66 km^2 with a warm temperate humid climate and warm summers (Köppen–Geiger climate classification, Kottek et al., 2006). The annual precipitation ranges from 357 to 793 mm (mean 548 mm), mean annual air temperatures from 7.8 to 10.9°C (mean 9.8°C) (1990–2020, weather station Müncheberg, Deutscher Wetterdienst [DWD] 2022), and annual potential evapotranspiration (PET) from 650 to 700 mm (Smith, Tetzlaff, Gelbrecht, et al., 2020). Because of high intensity convective events, summer is usually wetter than winter, whereas winter precipitation is more frequent and less intense. Average annual snowfall in Demnitz is small ∼34 mm (2000–2009, Deutscher Wetterdienst [DWD], 2022), although in 2021 this was 61 mm (Deutscher Wetterdienst [DWD], 2022). Because of the dominance of ET, annual runoff coefficients are typically >15% at DMC, and storm events resulting in surface runoff and erosion are rare (Gelbrecht et al., 2005). Nevertheless, an increasing trend in heavy rainfall events (events with >30 mm d^{-1}; 1990–1999: 7; 2011–2020: 13, Deutscher Wetterdienst [DWD], 2022) as well as rising mean air temperature (1990–1999: 9.2°C; 2011–2020: 10.1°C, Deutscher Wetterdienst [DWD], 2022) have been observed over the last 30 years. Additionally, longer drought periods were observed, for example, 2018–2020 in the catchment (Kleine, Tetzlaff, Smith, Goldhammer, & Soulsby, 2021), and are predicted to become more common in the future across the region (Lüttger et al., 2011).

The DMC is a typical lowland catchment of the North German Plain with a long history of anthropogenic influence including historic wetland drainage and canalisation of the stream network to facilitate intense agricultural land use (>60%). The second major land use is forestry (35%). Only small fractions (∼4%) of the catchment are covered by urban settlements or remaining wetlands (Figure 1). The hydrogeological structure of the DMC is shaped by the last glaciation (about 10,000–15,000 years BP) (Gelbrecht et al., 2005). Unconsolidated sediments form the upper soil and aquifer layers (Gelbrecht et al., 2005) with luvisols being dominant in the north of the catchment (over ground moraines), whereas the south is characterised by gleysols (in low-lying areas) and arenosols (over sandy deposits) (Figure 1). This is reflected by land use, where the silt-rich luvisols are used for agriculture, whereas the highly permeable, freely draining sandy soils (arenosols) are forested (Figure 1). The shallow groundwater depths (∼0.5 to ∼3.5 m at the DMC in Winter, see Kleine, Tetzlaff, Smith, Dubbert, & Soulsby, 2021) allow for extensive groundwater and stream interaction. Consequently, groundwater contributes >75% of stream discharge (Smith, Tetzlaff, Gelbrecht, et al., 2020). At the altitude of our study sites, the groundwater level is around 3 m below soil surface depending on the season (see Figure 3d).

The DMC has been at the focus of many environmental studies as a long-term experimental site. In the late 1990s, Gelbrecht et al. (1998, 2005) focused on agricultural pollution, whereas more
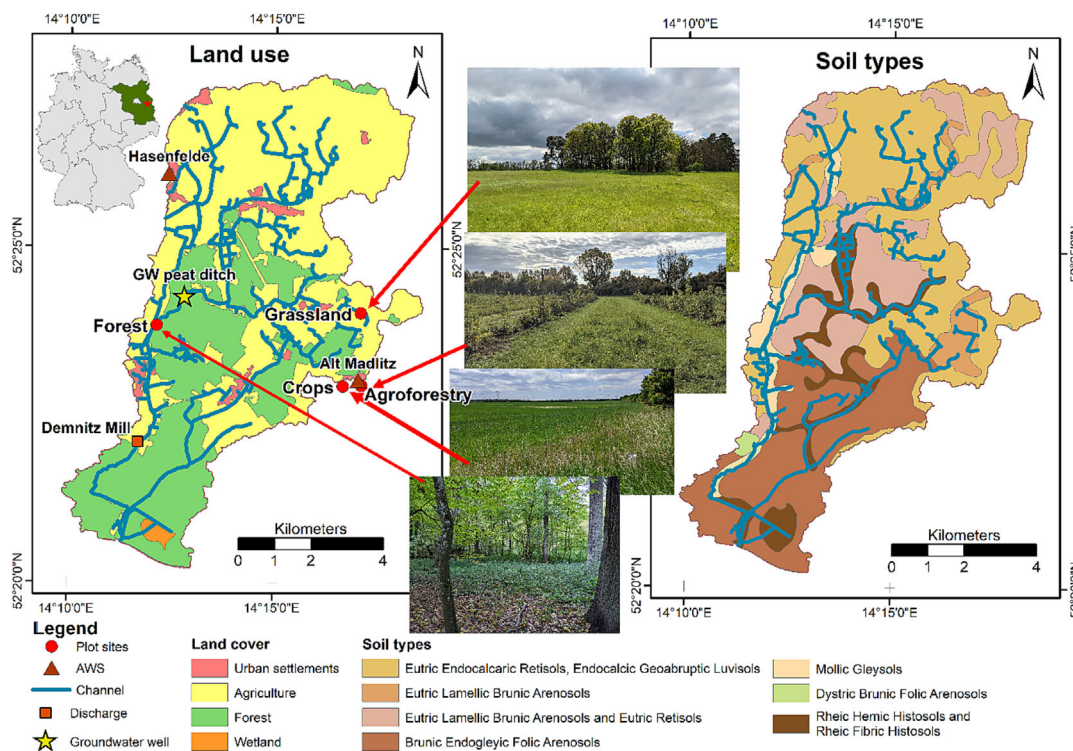

FIGURE 1 Study site area showing land use, plot sites, discharge, groundwater and weather stations (AWS) in the left panel and soil types in the right panel. The panel shows an overview map of Germany with Brandenburg highlighted in green and the position of the site by a red star in its upper left corner. Site photos provide representation of the modelled sites.

recent studies have concentrated on ecohydrological (Kleine et al., 2020; Kleine, Tetzlaff, Smith, Dubbert, & Soulsby, 2021; Kleine, Tetzlaff, Smith, Goldhammer, & Soulsby, 2021; Landgraf et al., 2022; Smith, Tetzlaff, Kleine, et al., 2020; Smith et al., 2021a, 2021b) and nitrate (Wu et al., 2022a, 2022b) fluxes. These investigations become especially important as the majority of agricultural land is not irrigated and forests contain a large proportion of shallow-rooted pine trees. Both are dependent on precipitation, its distribution and storage inside the soil and thus extremely sensitive to drought.

2.2 | Plot sites

We investigated four sites in the catchment with contrasting land uses at the plot scale. The sites are covered by forest, grassland, arable and an innovative mixed arable agroforestry scheme vegetation inhabiting the various soils of the catchment. All sites are located towards the latitudinal centre of the catchment with *Grassland*, *Agroforestry* (innovative arable) and *Crops* (arable) in the east and *Forest* in the west (Figure 1). *Agroforestry* and *Crops* are situated south from *Grassland* in close proximity to one another.

At the mixed deciduous-coniferous *forest* site, mature oak trees (*Quercus robur*) are dominant with other species like Scots pine (*Pinus sylvestris*), red oak (*Quercus rubra*) and Norway maple (*Acer platanoides*) occurring as well. The soil is covered by a relatively thick humus layer of ∼ 10 cm and followed by silty sand. With increasing depth, the soil becomes less silty (for detailed description of the sites' soil texture, see Kleine et al., 2021).

The *Grassland* is mostly inhabited by grass and some herbs (e.g. yarrow, *Achillea* sp.). At the northern edge of the site, a small tree shelter belt consisting of birch (*Betula* spp.) and aspen (*Populus tremula*) forms the border, though this did not shade the grassland under investigation (see Landgraf et al., 2022). The soil is characteristic of the retisols of the region with sandy and silty soil layers. It also contains small stone clasts up to 8 cm in diameter (see Landgraf et al., 2022).

The *Agroforestry* site is a combination of small deciduous trees or bushes (up to 2 m in height) planted in rows with legumes cultivated between. The rows are roughly 2–3 m apart and, though cultivated, are not irrigated. The land management shaping this site started in 2019. During 2021, no ploughing occurred but the legumes were mowed from 30 to 50 cm down to 10–20 cm a few times during growing season. Part of the legumes area was used as a free-range area for chickens at the last half of the year. The soil is a luvisol with sand content increasing with depth, and its structure was affected by mice burrows.

At the *crops* site, rye (*Secale cereale*) was cultivated in a conventional way without irrigation. Before spring, the site was ploughed and planted and harvested in mid-summer. After harvest, grass overgrew the site and was left over winter. The soil consists of luvisol which is silt-rich at the top and becomes sandier with increasing depth.

3 | METHODOLOGY

3.1 | Measurements and data

Precipitation amount, air temperature and relative humidity were monitored by two automatic weather stations (AWS) at Hasenfelde

and at Alt Madlitz (Figure 1). Devices used and their accuracy are detailed in Table S1 in the supporting information. We mainly used the hydroclimatic data measured at Alt Madlitz with data gaps being filled by Hasenfelde (∼5 to 10 km distance to study sites) or DWD data (Deutscher Wetterdienst, German Weather Service Müncheberg, ∼20 km distance to study sites Deutscher Wetterdienst [DWD], 2022). Data gaps of net radiation were assimilated from remote sensing products (ERA5-Land; Muñoz Sabater, 2019). Additionally, a mobile eddy covariance system (Li-COR Biosciences, Lincoln, NE, USA with LI 7500DS open path analyser, frequency 10–20 Hz, height: radiation 2 m and open path analyser 2.5 m; Smart Flux 3 system [Burba, 2013]) monitored climate at an open space area of the *Agroforestry* site. We used air temperature, precipitation amount, wind direction and speed, relative humidity, solar radiation, top soil latent heat flux, and top soil moisture to estimate ET. Although technical issues resulted in some calibration problems and data gaps, this gave a useful benchmark of the dynamics of measured ET. We also estimated PET via the FAO Penman–Monteith equation from the python package ETo (cf. Allen et al., 1998 for the method) at daily resolution (see Landgraf et al., 2022 for input parameters).

Leaf area index (LAI) was measured at *Forest* with a handheld device (LAI-2000 Plant Canopy Analyser) during soil sampling (referred to as *soil bag sampling*). Comparison of measured LAI with LAI extracted from the remote sensing product MODIS for *Forest* resulted in similar values (R^2 0.99, mean of R^2 for 27 variables, sd: 0.117). Hence, we chose the measured LAI with approximately monthly data for *Forest*, and remote sensing LAI at daily intervals for the other sites. For the remote sensing LAI, the following vegetation types were available: broad-leaved forest, conifer forest, pasture or cropland. We used pasture LAI as input data for *Grassland* and *Agroforestry* and cropland LAI for *Crops*. As pasture is grazed by livestock, its LAI is representative of a grassland, whereas the cropland LAI was representative for our crop site. For *Agroforestry*—being covered mainly by legumes and grass with narrow rows of small trees that are still establishing—we first simulated the site with all available LAI vegetation types as input data but found the LAI of pasture to be the best fit to simulate the measured soil water storage and isotopes.

Groundwater level was measured 4-hourly via a pressure sensor in the north of the catchment (Peat Ditch) and upstream of *Forest* (Figure 1) (Landgraf et al., 2022). Stream water level was monitored by the same pressure sensors at 'Demnitz Mill' (Figure 1). To convert water level into discharge, we used the rating curve by Smith, Tetzlaff, Gelbrecht, et al. (2020).

The top soils (0–10 cm) volumetric water content (VWC) was estimated at monthly intervals via a handheld device measuring the electric conductivity of the soil in mV, which was converted into VWC through calibration. For each site, we estimated means of the measurement replicas to gain top soil VWC. Below the top soil, permanently installed probes monitored soil VWC; *Forest* and *Grassland* soil pits had three depths (20, 60 and 100 cm). For *Forest*, we used the mean of two pits because of their proximity (∼15 m). At *Agroforestry* and *Crops*, probes were installed at 20, 40 and 80 cm (*Agroforestry*) or 15, 40, 60 and 100 cm (*Crops*). All data sets were aggregated into daily mean values with one VWC value per site and depth. As the soil moisture pit depths were not consistent with the depths of the model compartments (see below), the mean soil moisture for each depth of

the model was aggregated. For modelling, we converted volumetric soil water content (%) into soil water storage (mm).

All isotopic results given (precipitation, stream, soil water, groundwater and standards) are relative to the Vienna Standard Mean Ocean Water (VSMOW). Daily samples for stable water isotope analysis of precipitation were collected by a modified autosampler (ISCO 3700, Teledyne Isco, Lincoln, USA) equipped with a funnel positioned ∼1 m above ground level at the Hasenfelde AWS, including paraffin to prevent evaporation. Stream isotope samples were collected daily by an autosampler (ISCO 3700) similar to precipitation sampling (details of sampling in Landgraf et al., 2022), also with paraffin included within storage bottles. Groundwater was sampled monthly via a submersible pump (COMET-Pumpen Systemtechnik GmbH & Co. KG, Pfaffschwende, Germany). We stored all liquid samples (precipitation, stream and groundwater) at low temperatures (8°C) until analyses via cavity ringdown spectroscopy. Soil water isotopes were collected via bulk soil samples at the four sites during the growing season at five depths (0–5, 5–10, 10–20, 20–30, and 30–50 cm) on a 3- to 4-weekly basis. Samples were analysed via direct-equilibrium method (cf. Wassenaar et al., 2008) with an off-axis integrated cavity output spectroscopy (OA-ICOS) triple water vapour isotope analyser. Replicas were aggregated as means to gain single values per depth. Detailed description of the sampling and measuring of stable water isotopes can be found in Landgraf et al. (2022). The isotope results were aggregated to represent the model soil compartments with their according thickness. Statistics of the observed soil water storages and isotopes are given in Table 1.

3.2 | Model structure and development

The applied model is derived from the one-dimensional, plot-scale ecohydrological model *EcoHydroPlot* (see Stevenson et al., 2023 for full details). Briefly, the model simulates the ecohydrological partitioning of water into green and blue fluxes of evaporation (E), transpiration (Tr) and groundwater recharge (Re). The simulation of the model's water balance is conceptualised and based on canopy interception, surface runoff, soil infiltration, canopy and soil evaporation, transpiration, preferential vertical flow, percolation, and the groundwater recharge as a loss term (Figure 2). We used precipitation amount, PET and LAI at daily resolution of the calendar year 2021 as input data for the water balance. Additionally, our version of the model includes isotope tracking of deuterium (δ^2H) and is hereafter referred to as *EcoIsoPlot*. The processes for simulating stable water isotopes of the canopy and soil compartments include mixing of residual water with incoming water and evaporative fractionation of the canopy and upper soil compartment (Figure 2). To improve soil isotope simulations, we added another soil compartment resulting in the three soil compartments of *upper*, *lower* and *deeper* (0–10, 10–30 and 30–100 cm, respectively; Figure 2).

The model simulates canopy storage with precipitation inputs, evaporation loss, a maximum storage threshold, and resulting throughfall. Our version of the model simulates canopy storage with a slightly different workflow as Stevenson et al. (2023) as we had a different climatic setting, and this improved model simulations. Here, the available canopy storage was set as a maximum of interception storage and further limited by a throughfall threshold (if exceeded by interception storage, throughfall was allowed). Next, the available canopy storage was checked if changes in LAI reduced it below the current maximum storage. For the upper soil compartment, the model simulates net precipitation addition derived from throughfall, minus overland flow and preferential flow directed to the second layer. Outflows of the upper soil compartment are percolation, soil evaporation and transpiration. The lower soil compartment is regulated by percolation and preferential flow as inflow and transpiration and deeper percolation as outflow. The deeper soil compartment has deeper percolation as inflow and transpiration and groundwater recharge as outflow. For all soil compartments, the model estimates transpiration first until potential canopy transpiration is satisfied and allows evaporation if soil water storage is above the calibrated minimum (soil water storage range is used for calibration). Outflow below the simulated soil compartment is only allowed if inflow occurs and depends on soil conductivity via a nonlinearity parameter. Both are calibration parameters of the model.

TABLE 1 Summary statistics of observed soil water content and stable water isotopes of the three soil compartments in 2021. (SD = standard deviation).

| Site | Layer | Soil water storage mm | | | Soil water δ^2H ‰ | | |
		Min	Max	SD	Min	Max	SD
Forest	0 to 10 cm	7.53	26.28	7.03	−98.84	−29.01	3.14
	10 to 30 cm	8.78	50.40	11.88	−98.82	−44.28	5.18
	30 to 100 cm	34.13	135.10	34.04	−97.01	−49.32	4.35
Grassland	0 to 10 cm	5.66	28.87	5.82	−90.34	−22.31	4.00
	10 to 30 cm	9.49	44.86	10.44	−96.28	−41.67	4.13
	30 to 100 cm	58.96	101.22	11.17	−94.99	−48.97	4.99
Agroforestry	0 to 10 cm	10.40	32.06	7.77	−91.78	−21.85	2.55
	10 to 30 cm	9.92	49.78	11.03	−106.31	−47.70	3.19
	30 to 100 cm	108.84	213.90	35.58	−101.65	−57.13	5.26
Crops	0 to 10 cm	11.54	28.71	5.69	−86.44	−22.62	3.51
	10 to 30 cm	9.06	55.70	13.49	−101.81	−48.24	3.30
	30 to 100 cm	161.63	221.13	19.22	−103.18	−50.12	3.90
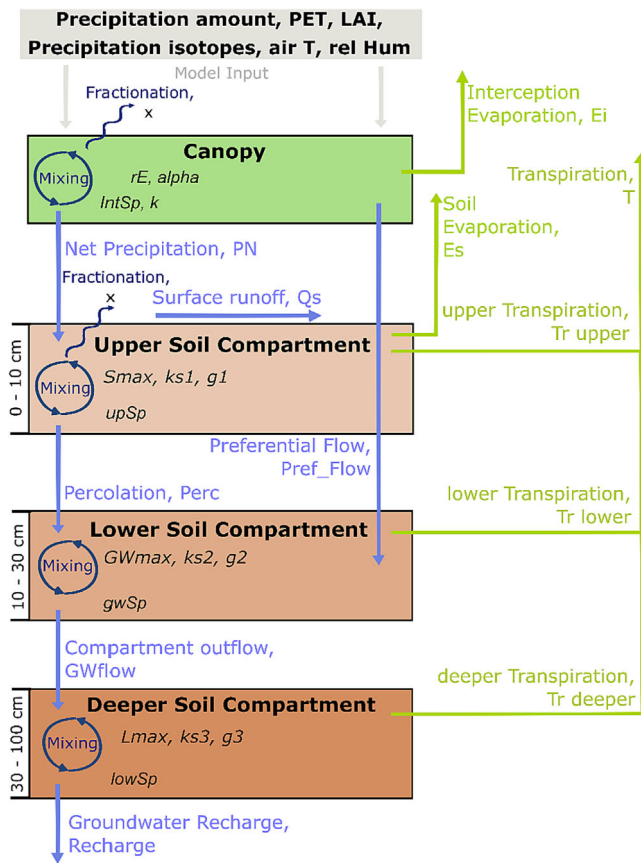
FIGURE 2 Conceptual diagram of the model showing the input data (PET: potential evapotranspiration; LAI: leaf area index; air T: air temperature; rel hum: relative humidity), compartments and the modelled processes. Water fluxes are divided into blue and green water fluxes according to coloration. Parameters of the model are included in their respective compartments and denoted in black.

Further, a throughfall threshold volume (TF; which if exceeded by interception storage, throughfall was allowed) was set and a preferential flow threshold volume (PFT; minimum net precipitation amount required to allow rapid preferential flow to depth) was estimated by Equation 6 (Table 2). In total, we used 13 water balance parameters (Table 2, Figure 2) with additional six isotope model parameters for calibration. For isotope tracking, the model requires inputs of precipitation isotopic composition (δ^2H; for model simplicity, only one isotopologues was used), air temperature, and relative humidity at daily resolution. The isotope tracking addition of the model consists of mixing processes of residual and incoming water as well as fractionation because of evaporation. We estimated the isotopic mixing during storage mixing via inflow and outflow of the compartment and assumed complete mixing for each layer.

We set (using observed values) or estimated initial values (e.g. means) for interception and soil water storage as well as isotopic composition (Table 2). The following parameters for isotope fractionation were calculated within the model (Table 2): fractionation factor at equilibrium (αe_H) (Horita & Wesolowski, 1994), equilibrium fractionation factor with permille notation (epse$_H$), kinetic fractionation factor (epsk$_H$) (Merlivat, 1978), precipitation–equilibrium assumption (Idl$_H$) (Gibson et al., 2008), enrichment slope (m$_H$) (Gibson et al., 2016) and limiting δ^2H (dstar$_H$) (Gonfiantini, 1986).

The initial values of interception were estimated via Equations 1 and 2 (Table 2) for storage and isotopes, respectively. For soil water storage, the starting values were equal to the first soil water content measurements (Table 2). As the first measurements for soil water isotopes were atypical and strongly influenced by snowmelt, we determined it was most effective to set the initial values as means per soil compartment (Table 2). As the different sites were similar in their isotopic compositions, the means were standardised. Estimation of surface cover fraction (SCF), interception storage and evaporation, net precipitation, preferential flow, soil water storage and transpiration (upper and lower soil compartment, as EcoHydroPlot only contained two soil compartments), and soil water evaporation (upper soil compartment) are explained in detail in Stevenson et al. (2023). Our *EcoIsoPlot* version of the model further included Hortonian overland flow, use of three soil compartments as opposed to two and stable water isotope tracking of interception and soil water storage (Table 3). Overland flow was allowed if net precipitation exceeded maximum infiltration capacity (parameter retained during calibration).

3.3 | Model calibration and evaluation

The model was applied to each site using data from 2021, with this data looped once for spin-up as previous work had shown this to be optimal for initialising storages (Stevenson et al., 2023). Initial parameter ranges were guided by field experience and monitoring. For each model run, we used Latin Hypercube sampling to generate 100,000 parameter sets within the defined parameter ranges (LatinHyper function, FME package in R; Soetaert & Petzoldt, 2010). Simulations were evaluated using the modified Kling–Gupta efficiency (KGE) (Kling et al., 2012), as well as the mean absolute error (MAE) of observed versus simulated soil water isotope values. Finally, each model output was checked after each run to ensure improvements in these quantitative metrics were not at the cost of unrealistic simulations in other areas of the model.

During initial calibration, we principally focussed on soil moisture KGEs of the three compartments for evolving the parameter ranges, given isotope simulations were less sensitive at this stage. After the parameter ranges of each vegetation type had been constrained to a point where further refinement resulted in worsening model performance, the global (e.g. calculated from all vegetation types) minimum and maximum value for each parameter was identified and used to define the initial parameter range then applied to each site (Table 4).

Next, this parameter range was further refined (independently for each vegetation type) by retaining only those parameter sets generating simulations in the 0.6 and above quantile for both soil moisture and isotope KGE values. Finally, the overall mean average of KGE values for all soil moisture and isotope data from all compartments were calculated, with the best performing 100 retained for final simulations. This approach ensured only parameter sets which gave, on average, the best simulations across the model domain were retained—with this process repeated independently at each site. This resulted in the final parameter ranges shown in Table 5, and the KGEs of soil moisture and isotopes in Table 6.

TABLE 2 Overview of initial, threshold and calculated parameters.

Start or threshold parameters	Site	Input value	Equation
Interception storage	All		1) $\alpha * LAI[1] * 0.5$
Upper soil water storage	Forest	20.3 mm	
	Grassland	15.5 mm	
	Agroforestry	26.8 mm	
	Crops	26.5 mm	
Lower soil water storage	Forest	36.6 mm	
	Grassland	33.3 mm	
	Agroforestry	38,8 mm	
	Crops	45.9 mm	
Deeper soil water storage	Forest	86.3 mm	
	Grassland	85.8 mm	
	Agroforestry	196,6 mm	
	Crops	194.1 mm	
Interception storage δ^2H (Int$_H$)	All	−58 ‰	2) $Int_H = \frac{\sum Precipitation\ \delta^2 H[1:365]}{365}$
Upper soil water δ^2H (STO$_H$)	All	−52 ‰	3) $STO_H = \frac{\sum Upper\ soil\ \delta^2 H[1:n]}{n}$
Lower soil water δ^2H (GW$_H$)	All	−66 ‰	4) $GW_H = \frac{\sum Lower\ soil\ \delta^2 H[1:n]}{n}$
Deeper soil water δ^2H (Low$_H$)	All	−70 ‰	5) $Deeper_H = \frac{\sum Deeper\ soil\ \delta^2 H[1:n]}{n}$
Throughfall threshold, TF	All	4.5 mm	
Preferential flow threshold, PFT	All	4.2 mm	6) $PFT = quantile(P[i:365], 0.9)$

Calculated parameters	Equation
Fractionation factor at equilibrium	7) $\alpha e_H[i] = \exp\left(\frac{1}{1000} * \left(\frac{1158.8 * Tk[i]^3}{10^9} - \frac{1620.1 * Tk[i]^2}{10^6} + \frac{794.84 * Tk[i]}{10^3} - 161.04 + \frac{2.9992 * 10^9}{Tk[i]^3}\right)\right)$
Equilibrium fractionation factor	8) $epse_H[i] = (\alpha e_H[i] - 1) * 1000$
Kinetic fractionation factor	9) $epsk_H[i] = 0.9755 * (1 - 0.9755) * 1000 * (1 - RH[i])$
Precipitation–equilibrium assumption	10) $Idl_H[i] = \frac{-58.7 - k * epse_H[i]}{1 + k * epse_H[i] * 10^{-3}}$
Enrichment slope	11) $m_H[i] = \frac{RH[i] * Idl_H[i] + epsk_H[i] + epse_H[i]/\alpha e_H[i]}{1 - RH[i] + epsk_H[i] * 10^{-3}}$
Limiting δ^2H	12) $dstar_H[i] = \frac{RH[i] * Idl_H[i] + epsk_H[i] + epse_H[i]/\alpha e_H[i]}{RH[i] - (epsk_H[i] + epse_H[i]/\alpha e_H[i]) * 10^{-3}}$

Note: Initial parameters were set as starting values (i.e. first timestep) for the simulations and constrained by the following model equations, whereas threshold parameters were set to a value limiting certain processes or fluxes without being edited during model simulation. Calculated parameters were set at the beginning of the model process and calculated for each simulated timestep directly. LAI, leaf area index.

4 | RESULTS

4.1 | Hydroclimate

The hydroclimatic conditions of the study year are shown in Figure 3 and were characterised by relatively high PET rates (>5 mm d^{-1} for 47 days), an unusually large storm event in summer (with ∼10% total precipitation) and a strong snow-influence in winter, which provided widely varying hydrological conditions in which to test the model. The year started with snow in February and afterwards it was relatively dry from February to April with ∼100 mm of precipitation during those months. The following summer was relatively wet with a notably large summer convectional storm event of ∼60 mm in June. Total precipitation in 2021 was 545 mm, and mean annual air temperature was 9.5°C. Relative humidity was highest in winter (100%) and lowest in summer before the mid-summer storm event (45%). PET was low at the beginning and end of the year and peaked during June, with an annual sum of ∼870 mm. Groundwater levels on the DMC catchment showed seasonal variability of ∼50 cm with a maximum in mid-March and minimum in November ranging between ∼270 and ∼320 cm below the ground surface, respectively. Streamflow generally

correlated with seasonal changes in groundwater levels and was highest in winter following rainfall events, with the stream drying up in July until flow recommenced in November.

4.2 | Simulating soil storage dynamics

Both the seasonal and storm event scale dynamics of the soil water storage in all soil compartments were generally well captured for all vegetation covers (Table 6). Only *Grassland* showed a slight offset between simulated and measured soil water storage in the deeper soil compartment from April onwards with lower KGEs (Figure 4). Soil moisture was highest at *Crops* and lowest at *Forest*, and at all sites, water content increased with increasing depth (Table 1). Observed means of soil water storage for all sites during the study were 15 mm in the upper, 28 mm in the lower and 82 mm in the deeper soil compartments. Fluctuations were highest in the upper soil compartment and were attenuated with increasing depth, with reduced variability in the simulated soil water storage compared to the monitored data. Soil water storage of the upper soil compartment was simulated best for *Crops* and *Grassland*. The drying of the lower soil compartment from

TABLE 3 Model stores and fluxes.

Water balance addition Stores and fluxes	Meaning	Equation
Overland flow	Surface runoff, if net precipitation larger infiltration capacity (Ic)	13) $Qs[i] = PN[i] - Ic$
Deeper soil transpiration	Transpiration if demand and if deeper soil water storage above minimum	14) $Tr_{deeper}[i] = (T_p[i] - Tr_{upper}[i] - Tr_{lower}[i]) * \left(\frac{Sdeep[i]}{L_{max}}\right)$
Groundwater recharge	Water percolating deeper layer into groundwater	15) $Recharge[i] = ks_3 * \left(\frac{Sdeep[i]}{L_{max}}\right)^{g_3}$

Isotope fluxes and mixing stores Stores and fluxes	Meaning	Equation
Initial interception storage	Interception storage before precipitation, evaporation	16) $Int_D[i] = I[i] - D[i] + E_i[i] + Th[i] + Int_{Sp}$
δ^2H interception reservoir	Mixing initial interception storage, precipitation	17) $Int_{CD}[i] = \frac{(Int_D[i]*Int_{CD}[i-1])+(D[i]*upP_{CD}[i])}{Int_D[i]+D[i]}$
Residual liquid interception storage	Defined by enrichment slope, limiting isotopic composition	18) $Idl_H[i] = (Int_{CD}[i] - dstar_H[i]) * (1-x)^{m_H[i]} + dstar_H[i]$
Fractionated δ^2H interception reservoir	Interception evaporation → fractionation of residual liquid; effects interception storage δ^2H	19) $fInt_{CD}[i] = (Int_D[i] * Int_{CD}[i]) - \frac{E_i[i]*Idl_H[i]}{Int_D[i]}$
Initial upper soil storage	Upper soil water storage before precipitation, evaporation, transpiration, percolation	20) $upSTO_D[i] = STO[i] - (P[i] - D[i]) - Th[i] + E_s[i] + Tr_{upper}[i] + Perc[i] + sto_{Sp}$
δ^2H upper soil storage	Mixing initial upper soil storage, infiltrated precipitation	21) $upSTO_{CD}[i] = \frac{(upSTO_D[i]*upSTO_{CD}[i-1])+(Th[i]*fInt_{CD}[i])+((P[i]-D[i])*upP_{CD}[i])}{upSTO_D[i]+P[i]-D[i]+Th[i]}$
Residual liquid upper soil storage	Defined by enrichment slope and limiting δ^2H	22) $Sdl_H[i] = (upSTO_{CD}[i] - dstar_H[i]) * (1-x)^{m_H[i]} + dstar_H[i]$
Fractionated δ^2H upper soil storage	Soil evaporation → fractionation residual liquid; effects upper soil water δ^2H	23) $fupSTO_{CD}[i] = (upSTO_D[i] * upSTO_{CD}[i]) - \frac{E_s[i]*Sdl_H[i]}{upSTO_D[i]-E_s}$
Initial lower soil storage	Lower soil water storage before percolation, preferential flow, transpiration, compartment outflow	24) $gwSTO_D[i] = GW[i] - Perc[i] - Pref\_Flow[i] + Tr_{lower}[i] + GWflow[i] + gw_{Sp}$
δ^2H lower soil storage	Mixing initial lower soil water, infiltrated percolation, preferential flow	25) $gwSTO_{CD}[i] = \frac{(gwSTO_D[i]*gwSTO_{CD}[i-1])+(Perc[i]*upCQ_D[i])+((Pref\_Flow[i])*upP_{CD}[i])}{gwSTO_D[i]+Perc[i]+Pref\_Flow[i]}$
Initial deeper soil storage	Deeper soil water storage before compartment inflow, transpiration, groundwater recharge	26) $lowSTO_D[i] = Sdeep[i] - GWflow[i] + Tr_{deeper}[i] + Recharge[i] + low_{Sp}$
δ^2H deeper soil storage	Mixing initial deeper soil water, infiltrated inflow	27) $lowSTO_{CD}[i] = \frac{(lowSTO_D[i]*lowSTO_{CD}[i-1])+((GWflow[i])*gwCQ_D[i-1])}{lowSTO_D[i-1]+GWflow[i]}$

Note: We only describe equations not present in the approach by Stevenson et al. (2023). Equations describe the water balance of the deeper soil compartment and the stable water isotope simulation which includes water balance recalculation required for mixing simulation.

May until the mid-summer storm event end of June was captured less well as soil storage was underestimated at the sites except *Crops*. All sites responded strongly to the storm event and simulations matched the resulting increase of the observed soil water storage well at the lower soil compartment. Although the peak of the mid-summer storm in the deeper soil compartment was simulated damped compared to observations, still, in general, the damped seasonality of the deeper soil compartment was captured well by the model.

4.3 | Simulated isotope dynamics

Soil water isotopic dynamics were captured generally well with dynamics in the deeper compartment captured best, with slightly depleted results for the simulations of the upper and lower

compartment compared to monitored data (Figure 5 and Table 6). The upper soil compartment isotopic composition is simulated by mixing of residual and incoming water, and also by fractionation. The latter is related to soil evaporation. This evaporated, mixed water is what is assumed to be transported into the lower layer affecting its isotopic composition by mixing. At the beginning of the year, observed soil water isotopic composition was depleted in heavier isotopes because of snow, which was reflected well in the simulations (Figure 3a). During the year, stable water isotopes in the upper soil were enriched in heavier isotopes because of summer rainfall inputs and the effects of evaporative fractionation, with a mid-summer storm event resetting the evaporative signal. The resetting is not evident from our plots, but it was obvious in the study from Landgraf et al. (2022) where lc-excess data are also estimated (see Figure S1). The event equalised the

TABLE 4 Calibrated parameters in the model.

Water balance Parameters	Meaning
rE	Extinction factor
α	Interception threshold parameter
Ic	Maximum infiltration capacity
PF_Scale	Preferential flow path parameter
Smax	Maximum soil moisture content upper soil compartment
ks1	Saturated hydraulic conductivity upper soil compartment
g1	Nonlinear scaling parameter upper soil compartment, if $g1 = 1$, linear case
GWmax	Maximum soil moisture content lower soil compartment
kfs2	Saturated hydraulic conductivity lower soil compartment
g2	Nonlinear scaling parameter lower soil compartment, if $g2 = 1$, linear case
Lmax	Maximum soil moisture content deeper soil compartment
ks3	Saturated hydraulic conductivity deeper soil compartment
g3	Nonlinear scaling parameter deeper soil compartment, if $g3 = 1$, linear case
Isotope tracking Parameters	**Meaning**
IntSp	Passive interception storage mixing volume
stoSp	Passive upper soil water storage mixing volume
gwSp	Passive lower soil water storage mixing volume
lowSp	Passive deeper soil water storage mixing volume
k	Seasonality factor Craig–Gorden model
x	Water vapour mixing ratio Craig–Gorden model

isotopic composition of the monitored soils at all sites except *Forest* and disturbed the hysteresis cycle (Landgraf et al., 2022). This was simulated especially well in the lower and deeper soil compartment. At the end of August and October, increasingly depleted isotopic inputs from precipitation events resulted in depletions of heavier isotopes in soil water which were captured well by the simulations. At *Forest*, isotope signatures of the deeper soil compartment showed highest variability, whereas at *Agroforestry*, we found lowest variability (Table 6).

4.4 | Dynamics in ecohydrological fluxes

The general partitioning of green and blue water fluxes was plausibly simulated with model estimations allowing us to quantify differences in fluxes of transpiration, interception evaporation, soil evaporation, overland flow and recharge between the contrasting land covers (Table 7). Green water fluxes directing water back to the atmosphere were highest at *Forest*, whereas blue fluxes contributing to groundwater recharge were highest at *Grassland* (Table 7). Transpiration and overall evaporation (sum of interception and soil evaporation) were highest at *Forest* and *Agroforestry*, whereas recharge was highest at *Grassland* and *Crops* (Figure 6). Both of the latter were overlapping in

terms of their water partitioning dynamics. Comparing partitioning results for solely soil moisture KGE selection with combined soil moisture and isotope KGE selection, *Forest* deviated more from the other sites by only considering soil moisture KGEs as it showed even less recharge in those estimations (Figure 6). Temporal partitioning of water fluxes may be found in Figure S2 and shows that soil evaporation is higher in winter and spring until leaves are fully developed at the end of May when interception becomes the dominant evaporative loss, particularly under forest.

Cumulative totals of simulated ET were less than half of those of PET (Figure 7). This can be explained by PET commonly being higher than *actual* ET when soils are drier and cannot sustain atmospheric moisture demand (Anabalón & Sharma, 2017). Although PET data were derived from Hasenfelde, a station set 5-10 km further North in the catchment, it's proximity to settlements (houses and streets) with less forest around than the monitored sites possibly resulted in greater rates of PET than our modelled sites. Still, Hasenfelde was the closest weather station with reliable complete time-series. Finally, given the relatively simple structure of the model, it is likely that the decrease in simulated ET when soils experienced more substantial drying was not fully representative of the actual ET occurring because of the shallow evaporative front of 10 cm in the model.

Recharge was highest in spring and lowest in September and October. *Grassland* had the highest recharge, and *Forest* had the lowest (Figure 8). Recharge effectively "shut down" in June, except at *Crops*, where recharge continuously increased following summer rainfall and caught up with *Grassland* levels (Figure 8). Comparing normalised groundwater level and simulated recharge, we found those were similar, with a short time lap between normalised simulated recharge (faster) and normalised groundwater level (Figure 9). During a dry phase between August and November, the normalised groundwater-level curve had a steeper slope than normalised simulated recharge (Figure 9).

5 | DISCUSSION

5.1 | Modelling land use-induced evaporation and transpiration

Different vegetation covers can result in different water fluxes depending on the effects of energy partitioning (resulting in ET variations; Moore & Heilman, 2011) and precipitation partitioning (Friesen & Van Stan, 2019). The model captured well the observed differences in soil moisture between the sites (Landgraf et al., 2022), and, given soil moisture acted as a constraint in ET simulations, provided confidence in ET simulations which increased volumetrically in the order Grassland < Crops < Agroforestry < Forest. Nonetheless, some uncertainty was present (Figure 6) being greatest at the Forest site because of its heterogeneity in soil (e.g. thickness of humus layer) and vegetation (e.g. various tree species with different life stages). The importance of canopy and rooting densities in transpiration was evident at the grassland site, which had the lowest transpiration, as has been observed elsewhere (Douinot et al., 2019; Liu et al., 2021). Conversely, simulated ET was greatest at the Forest and Agroforest sites because of the denser canopies and deeper rooting systems resulting in higher interception and transpiration (Moore & Heilman, 2011; Wang et al., 2017).

TABLE 5 Initial and final parameter ranges of parameters used for calibration of all vegetation types.

Parameters		rE -	Alphamm	Smaxmm	lcmm	ks1 (per day)	ks2 (per day)	ks3 (per day)	GWmaxmm
Initial calibration	min	−0.33	2	45	40	5	6	6	50
	max	−0.1	5	135	60	18	20	20	90
Forest final	min	−0.33	2	60	40	8	6	10	50
	max	−0.2	3	85	52	18	18	20	90
Grassland final	min	−0.33	2.25	70	50	10	12	15	50
	max	−0.25	3	100	60	16	16	18	80
Agroforestry final	min	−0.33	3	80	45	6	7	16	70
	max	−0.2	4.5	110	57	8	12	18	90
Crops final	min	−0.33	2	120	50	6	8	8	60
	max	−0.25	2.8	135	60	10	10	14	85

TABLE 5 (Continued)

Parameters		Lmaxmm	g1-	g2-	g3-	PF_Scale-	INTpmm	stoSpmm	gwSpmm	lowSpmm	k-	x-
Initial calibration	min	150	1.1	2	2	0.2	0.5	1	3	10	0.25	0.25
	max	460	3.5	4	5.5	0.9	1	20	40	100	0.9	0.75
Forest final	min	150	2	2	2	0.4	0.8	10	20	50	0.25	0.25
	max	280	3	4	5.5	0.8	1	20	40	100	0.9	0.75
Grassland final	min	150	1.8	3	3	0.55	0.5	10	20	60	0.25	0.25
	max	250	2.3	3.5	4	0.65	1	20	40	100	0.9	0.75
Agroforestry final	min	330	1.5	2	3	0.6	0.5	3	5	80	0.25	0.25
	max	420	2.2	3.5	4.4	0.8	1	10	20	100	0.9	0.75
Crops final	min	300	1.4	3	3.2	0.6	0.5	5	5	5	0.25	0.5
	max	450	1.75	3.75	4.7	0.85	1	10	20	20	0.5	0.75

TABLE 6 KGEs for soil water storage and deuterium based on observed value against minimum-, mean- and maximum-simulated value and confidence bounds.

Soil water storage									
Vegetation	Upper soil minimum (—)	Upper soil mean (—)	Upper soil maximum (—)	Lower soil minimum (—)	Lower soil mean (—)	Lower soil maximum (—)	Deeper soil minimum (—)	Deeper soil mean (—)	Deeper soil maximum (—)
Forest	0.79	0.79	0.60	0.75	0.88	0.80	0.66	0.90	0.79
Grassland	0.69	0.83	0.85	0.72	0.84	0.87	0.26	0.28	0.28
Agroforestry	0.74	0.82	0.79	0.82	0.89	0.86	0.77	0.84	0.84
Crops	0.72	0.70	0.61	0.62	0.68	0.72	0.59	0.68	0.62
Soil water δ^2H									
Vegetation	Upper soil minimum [—]	Upper soil mean [—]	Upper soil maximum [—]	Lower soil minimum [—]	Lower soil mean [—]	Lower soil maximum [—]	Deeper soil minimum [—]	Deeper soil mean [—]	Deeper soil maximum [—]
Forest	0.57	0.63	0.66	0.62	0.67	0.73	0.66	0.69	0.77
Grassland	0.69	0.71	0.73	0.69	0.70	0.70	0.71	0.71	0.73
Agroforestry	0.73	0.75	0.77	0.77	0.73	0.74	0.76	0.76	0.77
Crops	0.68	0.70	0.72	0.67	0.67	0.64	0.59	0.60	0.66

Compared to soil moisture, the isotopic composition of soil water was less affected by land use, possibly because of relatively wet conditions of the study year of 2021 resulting in less distinct variability of ET (Andréassian, 2004; Hasselquist et al., 2018). Looking at ET variability, a study from Canada found deciduous trees and croplands to be transpiration dominated (Gibson et al., 2021). Our simulations were transpiration dominated, considering the whole year (Figure S2). However, winter was evaporation dominated, and the transition from soil evaporation to transpiration dominated occurred for most sites around April and for *Forest* roughly 1 month later in May following leaf-out and increasing LAI. In Figure S3, the monitored normalised forest sap flow suggests a delayed response in simulated transpiration of Forest as transpiration is directly correlated with sap flow rates (Wullschleger et al., 2001). However, the sap flow data are derived from evergreen pine trees nearby, whereas the site *Forest* mainly comprises deciduous trees resulting in a postponed rise of transpiration because of the absence of leaves early in the season. Importantly, the model captured those canopy differences. The ratio of simulated Tr/ET was highest at *Forest* (59%) and lowest at *Grassland* (56%), similar to previous studies (Ma et al., 2020; Schlesinger & Jasechko, 2014; Smith et al., 2021a; Zhou et al., 2016). This showed that *Forest* soil moisture was more strongly influenced by transpiration than evaporation, whereas at *Grassland*, evaporation plays a more important role (still, transpiration is the largest component of ET).

5.2 | Water partitioning of an evolving agroforestry site

Agroforestry being a mixture of forest and crops is described to have positive impacts on various aspects like farm productivity, environmental sustainability, and water conservation (Noordwijk, 2020; Rijal, 2019). However, the processes influencing the water dynamics via canopy or rooting structure are yet to be fully understood (Hasselquist et al., 2018). Striking are the simulation results of our *Agroforestry* site which fall between *Forest* and *Crops* results in our ET ternary plot (Figure 6). A study by Andréassian (2004) found flux

partitioning between crop/grassland and forest sites without deep-rooting system to have been mainly affected by canopy interception. We found that the *Agroforestry* site is similar to *Grassland* and *Crops* in terms of transpiration, interception evaporation and soil evaporation, whereas it is more similar to *Forest* in terms of recharge (Figures 6 and 8). These similarities with *Grassland*/*Crops* and other similarities with *Forest* may be caused by the canopy and deeper rooting system at *Agroforestry* being not fully developed yet (trees 2 m at max; Landgraf et al., 2022). This lack of canopy differences between *Agroforestry* and *Grassland* in the model may also be related to the LAI inputs, which are equal for both sites because of the lack of distinct agroforestry LAI. Still, it is likely that the *Agroforestry* site because of growing canopy and rooting system transitions into the direction of *Forest*, which was not clear by the isotope analysis of the previous study (Landgraf et al., 2022) but captured via our model.

5.3 | Modelling land use-induced differences in groundwater recharge

Understanding the impact of vegetation on the subsurface processes affecting groundwater recharge is crucial for managing groundwater as a resource (Owuor et al., 2016; Taylor et al., 2013). At the DMC, the *Grassland* site had the highest simulated recharge, whereas *Forest* recharge was lowest, like findings of Kleine et al. (2020) at DMC and Douinot et al. (2019) at Stechlin, some 100 km northwest. A global study by Kim and Jackson (2012) found recharge to be highest at cropland followed by grassland, woodland and shrubs. However, the study included irrigated cropland, whereas our crop site was non-irrigated. We found no major differences of simulated groundwater recharge for *Grassland* and *Crops*, whereas another study in Germany found transition from grassland to winter crops reduced GW recharge (Orlowski et al., 2016). Our *Crops* site was harvested in August and reverted to grass in the following months, whereas the cropland site of Orlowski et al.'s (2016) study remained cropland during winter, possibly explaining the differences. Nevertheless, this is an interesting finding as it shows that the EcoIsoPlot model captured those temporal
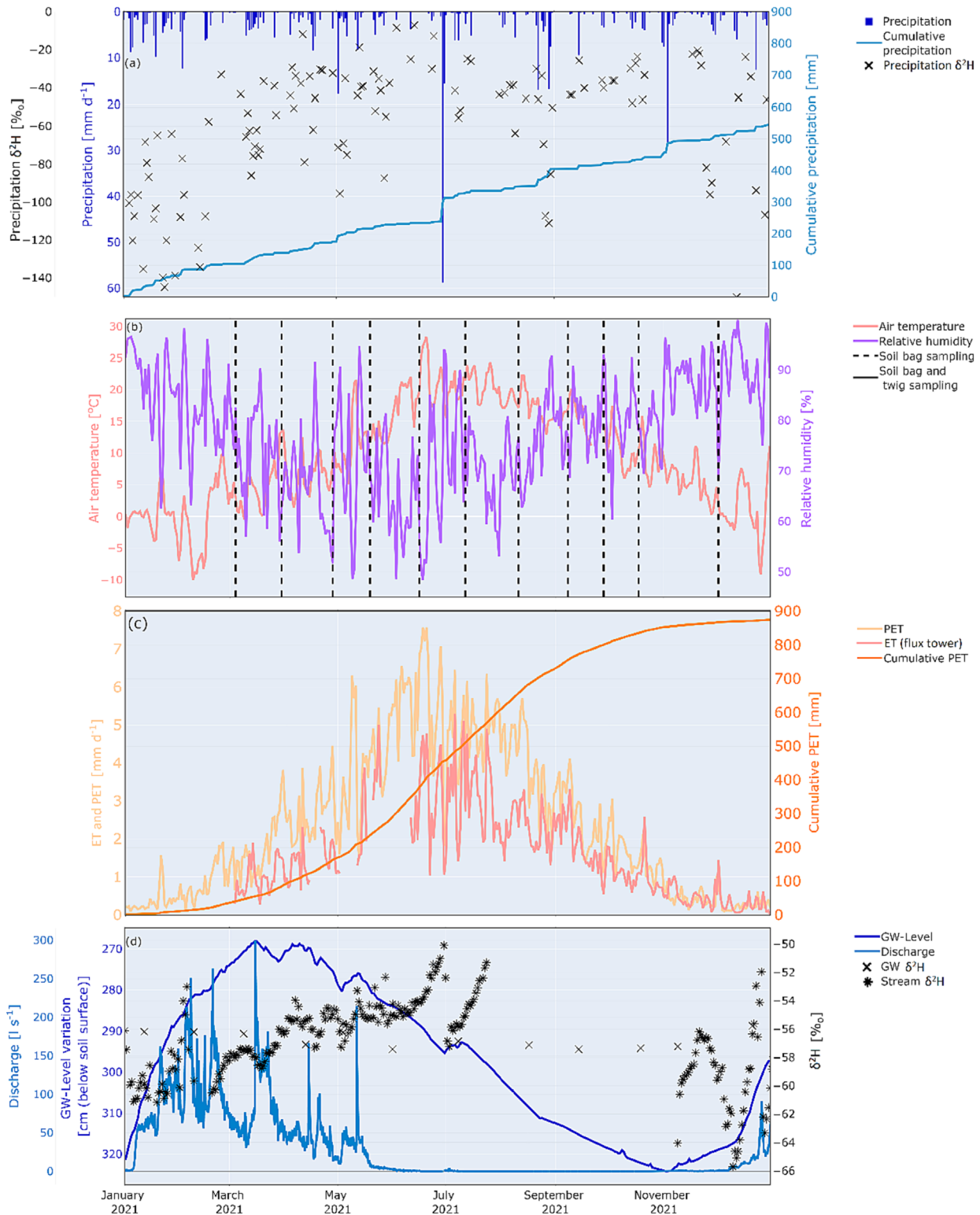
FIGURE 3 (a) Hydroclimatic conditions with precipitation daily amount, sum and δ²H; (b) air temperature, relative humidity, and sampling dates (vertical dotted lines); (c) ET and PET daily amount and PET sum; (d) groundwater level variation, discharge, groundwater, and stream δ²H (with data gaps when stream was not flowing). PET, potential evapotranspiration; ET, evapotranspiration.

changes in canopy characteristics. Water partitioning differences are also connected to soil properties (Geris et al., 2015), for example, sandy forest soils are highly conductive and lowest soil water content, whereas crop soils are more retentive (silt/clay), least conductive and highest soil water content maintaining water availability for ET (Landgraf et al., 2022). In general, the model structure successfully conceptualised those differences by calibration of the soil conductivity and nonlinear scaling parameters.

5.4 | Capturing key influence of ET processes in the critical zone

The parsimonious model simulated the multiple processes of water partitioning in the CZ, that is, evaporation (soil and interception), transpiration and groundwater recharge reasonably well, although absolute estimations may be improved. Overall, the storage dynamics were captured well, similar to process-based ecohydrological models
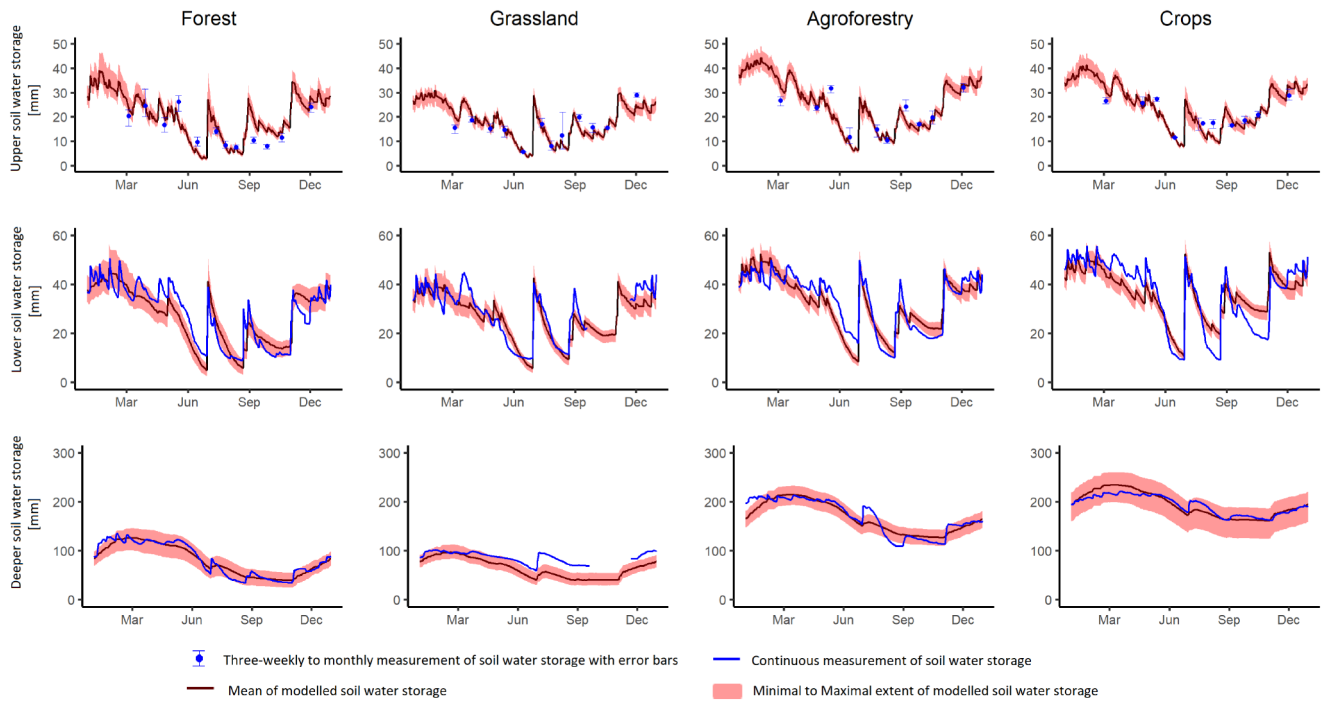
FIGURE 4 Soil water storage dynamics with measured and simulated (mean) results also representing the modelled range from minimum to maximum of the 100 best-performing simulations in the shading. Error bars of the data points represent minimum and maximum of the measured replicas.
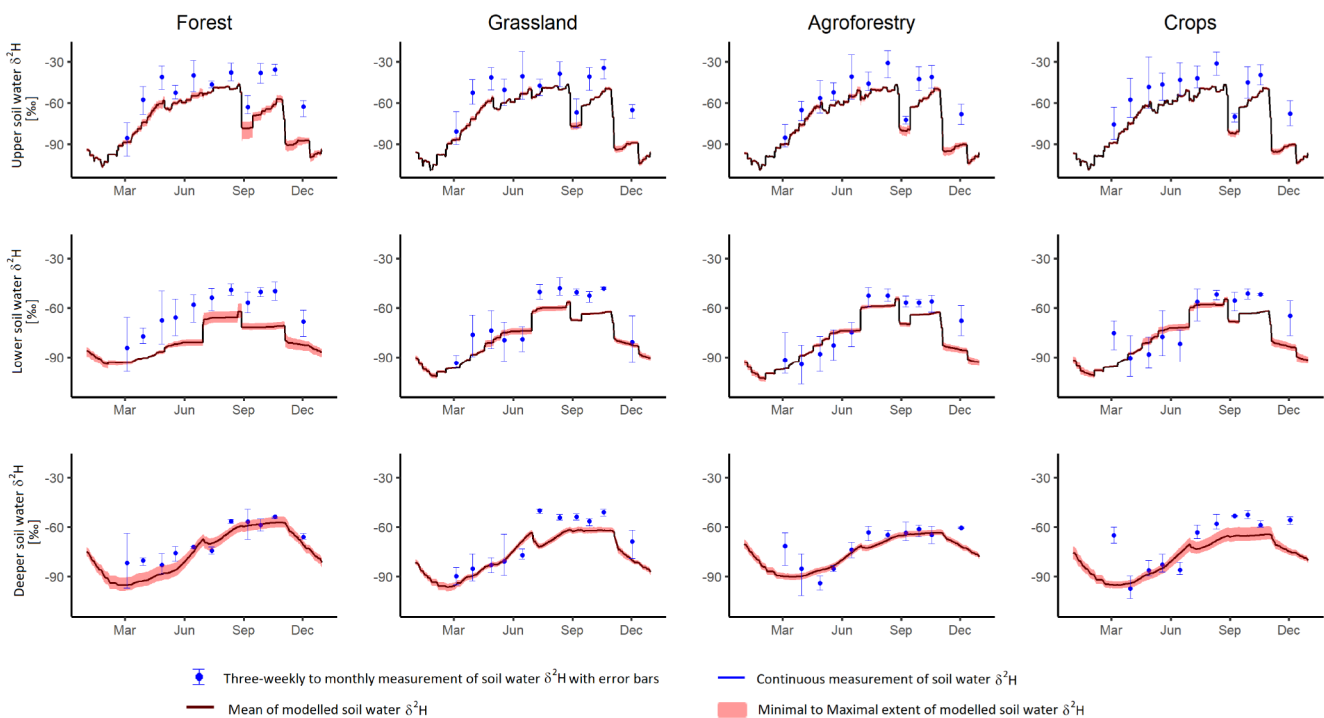
FIGURE 5 Soil stable water isotope dynamics with measured and simulated (mean) results also representing the modelled range from minimum to maximum of the 100 best-performing simulations in the shading. Error bars of the data points represent minimum and maximum of the measured replicas.

(e.g. Smith et al., 2022). Key water fluxes were simulated well and with reasonable values for the region, for example, ET higher than recharge (Douinot et al., 2019; Kleine, Tetzlaff, Smith, Dubbert, & Soulsby, 2021). Simulated overland flow was very small with only a few millimetres over the whole year as the area of the DMC is

relatively flat (average slope 2%, Smith, Tetzlaff, Gelbrecht, et al., 2020). The simulated ET dominated the water balance at the DMC (68–80% of precipitation) for the study year 2021. This is consistent with previous findings of ET at the DMC (83.7%; >80%) (Smith et al., 2021b; Wu et al., 2022a) and just higher than global ET

TABLE 7 Water balance of the different sites with final calibration showing mean and standard deviation (SD for PN: net precipitation, Qs: surface runoff, I: interception storage (after evaporation), Th: throughfall (included in net precipitation), Ei: interception evaporation, Tr: transpiration, Es: soil evaporation, recharge: outflow below deeper soil compartment, ET: evapotranspiration (sum of Ei, Tr, and Es), re + ET + Qs: total blue and green water fluxes (sum of ET, recharge and surface runoff).

Site		PN mm	Qs mm	I mm	Th mm	Ei mm	Tr mm	Es mm	Recharge mm	ET mm	Re + ET + Qs mm
Forest	Mean	264	13	144	17	107	258	69	114	435	561
	SD	23	3	39	3	4	14	9	10		
Grassland	Mean	287	1	31	1	83	208	80	174	371	546
	SD	8	1	4	0	3	8	5	7		
Agroforestry	Mean	273	5	51	4	94	246	82	122	422	550
	SD	9.5	3.1	5.8	1.0	2.8	5.6	3.9	5.5		
Crops	Mean	273	1	52	0	80	220	80	164	380	545
	SD	11.4	1.7	9.2	0.2	3.3	7.0	4.0	7.7		

Note: For comparison, annual observed precipitation was 545 mm.
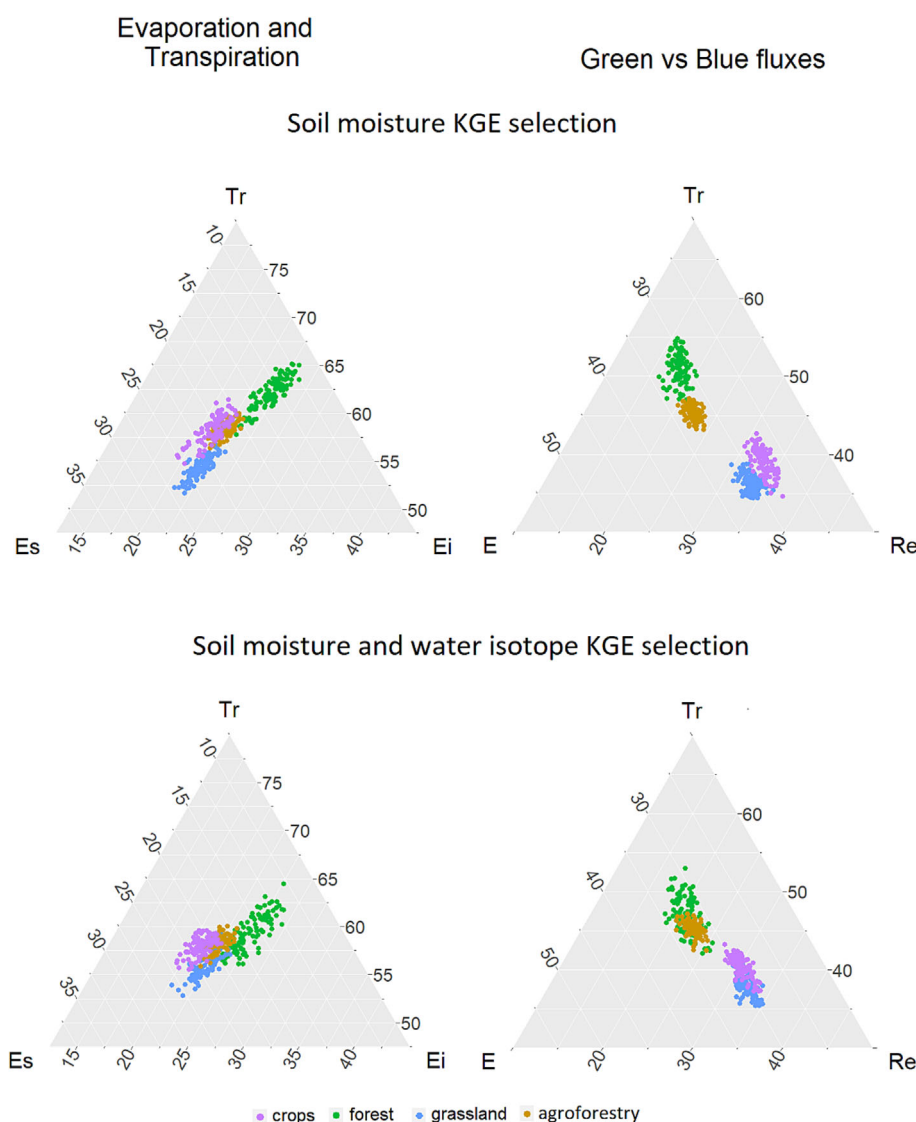
FIGURE 6 Shown are ternary plots for percentages of annual transpiration (Tr), soil (Es) and interception evaporation (Ei) on the left with plot ranges of 0.8 for Tr, 0.5 for Es and 0.45 for Ei. On the right ternary plots for percentage of annual transpiration (Tr), evaporation (E = Ei + Es) and recharge (re) are shown with ranges of 0.7 for Tr, 0.6 for E, 0.5 for Re. Each site is represented by 100 data points derived from the selected best-performing simulations considering soil moisture KGEs for the top plots and soil moisture and isotope KGEs for the base plots. KGEs, Kling–Gupta efficiency.

averages (about 60% of precipitation) (Jung et al., 2019). Simulated transpiration (38–47%), soil evaporation (13–15%) and interception evaporation (15–20%) results are also comparable to those from Smith et al. (2021b) (transpiration 49.8%, soil evaporation 9.4% and interception evaporation 24.4%) with soil evaporation being slightly higher and interception evaporation being slightly lower for our simulations. In general, simulated ET is lower than estimated PET. From model perspective, this might hint at flux underestimation by the model or limitations to support high ET demands by the upper soil compartment. However, annual PET of 870 mm in 2021 is relatively

FIGURE 7 Measured ET (flux tower), estimated PET and simulated ET (mean of 100 best-performing simulations) with sum curves for estimated PET and simulated ET. PET is derived from data at Hasenfelde; hence, site-specific ET may differ in magnitude because of potential overestimation at Hasenfelde. PET, potential evapotranspiration; ET, evapotranspiration.
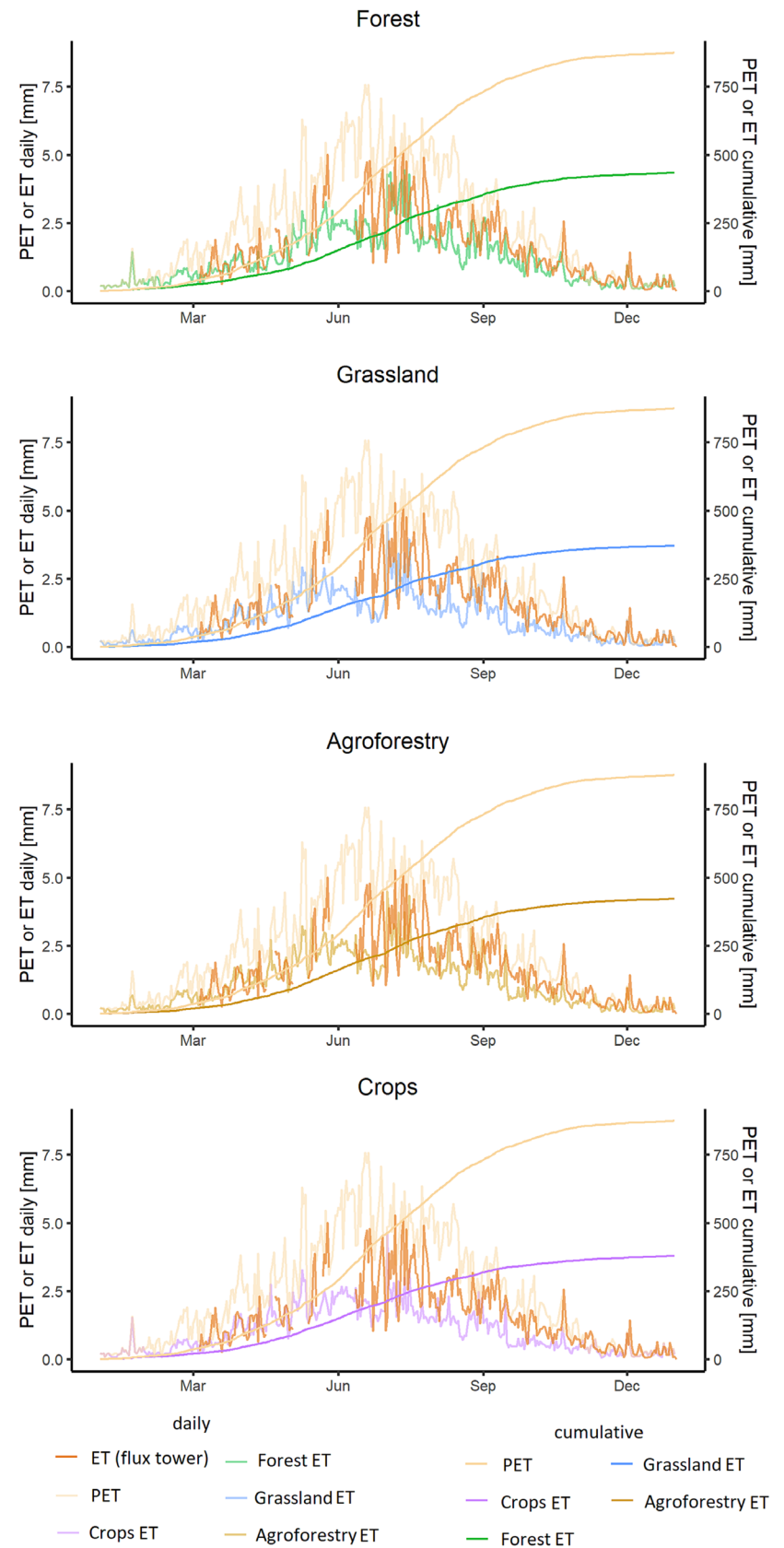
high for the DMC, which is described around 650–700 mm a^{-1} by Smith, Tetzlaff, Gelbrecht et al. (2020). Absolute values of ET are challenging to estimate, still our model stayed in ranges similar to previous studies and was able to capture ET variability which improves our understanding of ET flux changes.

5.5 | Capturing key influence of groundwater recharge in the CZ

The dynamics of simulated groundwater recharge at the DMC are good as shown by comparison with groundwater table fluctuation
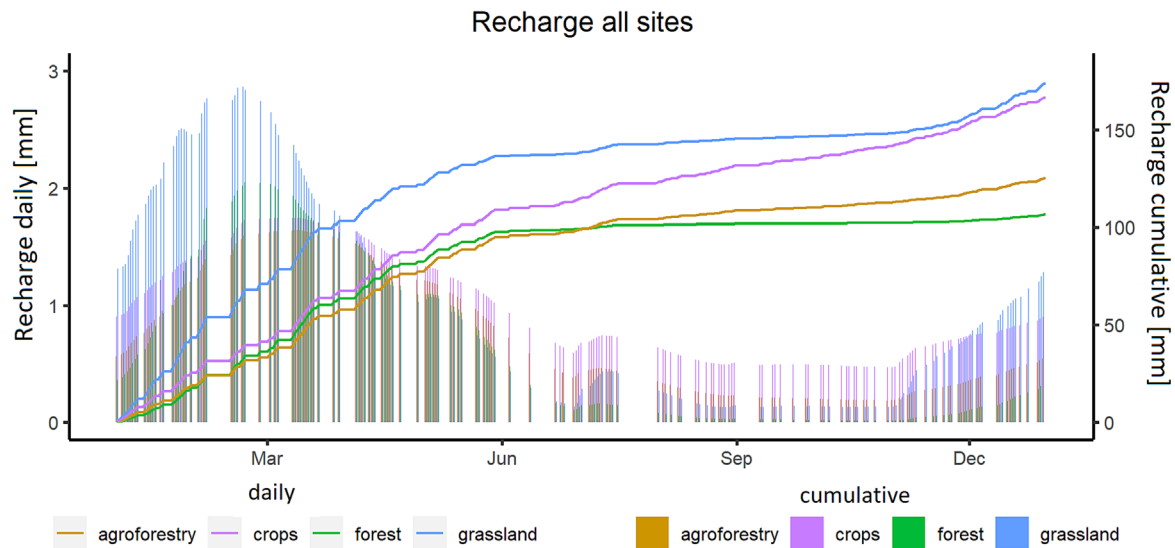
FIGURE 8 Simulated groundwater recharge (mean of 100 best-performing simulations of water losses from the bottom of the model domain) for each site and the cumulative sum.
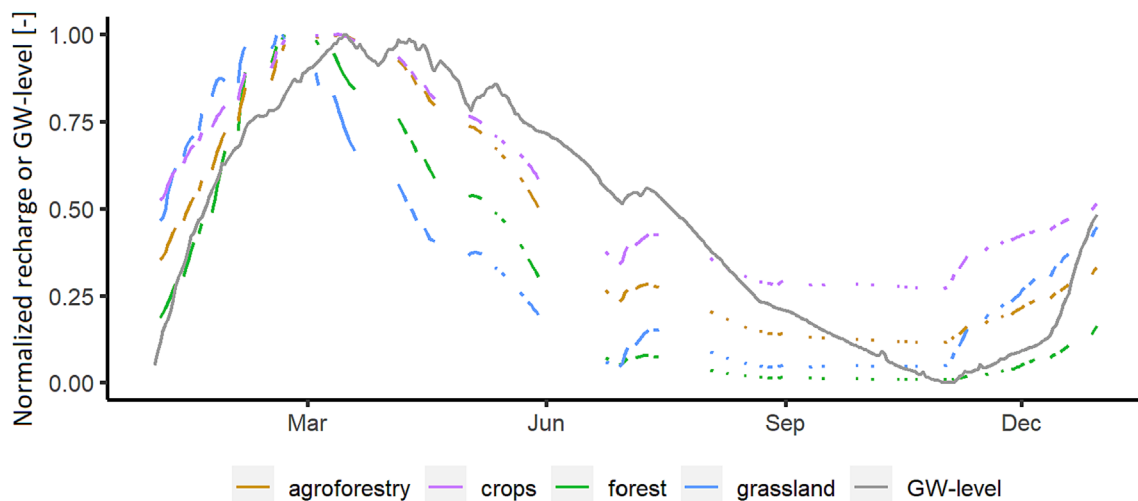
FIGURE 9 Normalised and simulated recharge of the study sites compared with normalised groundwater level of the groundwater well. Simulated normalised data equal to zero were set to NA.

reflecting the seasonality and episodicity (cf. Wu et al. 2019 for groundwater seasonality and episodicity). Simulated recharge varies between ∼ 21% and ∼32% of precipitation, which is higher than the findings of 18% at the DMC from Wu et al. (2022a) or 10% by Smith, Tetzlaff, Gelbrecht et al. (2020). Globally, ∼16% of precipitation contributes to groundwater recharge, although uncertainties because of data scarcity of several regions were pointed out (Jasechko et al., 2014; model from Wada et al. 2010). Another Germany wide study estimated a maximal possible recharge of 10–25% for the region of the DMC (Jankiewicz et al., 2005). It has to be considered that snow melt in the beginning of the year and the mid-summer storm event may have resulted in relatively high recharge, although the extent may be debatable. Nevertheless, the model captured those higher recharge results with possibly minor overestimation. Previous studies of the DMC found the catchment to be dominated by vertical flow (Kleine, Tetzlaff, Smith, Goldhammer, & Soulsby, 2021; Smith, Tetzlaff, Gelbrecht, et al., 2020). It may be valuable to consider here

that the model estimated soil water storage down to 1 m and outflow of the compartment base is assumed to be recharge, which may also refill the unsaturated zone (e.g. from 1 to 3 m below soil surface) or be accessed by roots instead of contributing to groundwater.

5.6 | Effects of integrating stable water isotopes into a lumped tracer-aided model

The study demonstrates that incorporating isotopes into a parsimonious tracer-based modelling approach provided an additional constraint on the process realism of water partitioning into blue and green water fluxes. Previous studies showed such parsimonious models to reflect water fluxes quite well (Soulsby et al., 2016; Stevenson et al., 2023). Integrating tracers into flux models helps identifying an appropriate structure (Vaché & McDonnell, 2006) and internal consistency of the model (Birkel et al., 2015). Here, we used

the most common concepts of state variables to quantify the tracer concentration of different CZ compartments in the soil, whereas tracer movement is controlled separately by flux and mixing equations (Birkel & Soulsby, 2015; Hrachowitz et al., 2016; Qi et al., 2022). The soil moisture simulations showed a higher goodness-of-fit than isotopes, although the higher resolution soil moisture data set had a greater information content and more commensurability than the monthly isotope measurements. Still, simulation of isotopic composition captured the dynamics well with good KGEs. If simulations were solely selected by soil moisture KGEs, the selected KGEs are slightly higher if adding isotope KGEs to the selection process. We also saw a better constraint in terms of partitioning as adding the stable water isotopes resulted in reduced spread of simulations (e.g. *Forest* and *Agroforestry* recharge). This means that model performance was slightly decreased, although process representation of the model was improved as the model covered two interacting processes (Birkel & Soulsby, 2015; Stadnyk & Holmes, 2020). During calibration, similar to a study by Smith et al. (2022), we found isotope KGEs improved with soil moisture performance. Others found a decrease in model parameter uncertainty by implementing stable water isotopes into a run-off model (He et al., 2019). In future studies, an improvement of our model may be the implementation of lc-excess to better capture E influences (see Smith et al., 2022; Sprenger et al., 2018). However, the quantitative estimations are more likely caused by structural limitations of the model (particularly the generic parameterisation of the Craig–Gordon equilibration and uncertainty over depth of the evaporating front). The good predictability of the isotopic composition may also be linked to the previously mentioned major storm event that probably acted like a tracer test, although resetting the evaporative signal (shown in Landgraf et al., 2022).

The simulated soil water isotopic composition at the upper and lower soil compartment was more depleted compared to the measurements. Possibly, the model underestimated soil evaporation, and hence, less fractionation was simulated. A study by Stumpp and Hendry (2012) used a one-dimensional equilibrium flow and transport model and found that snowmelt input was not represented in the simulated isotopic composition. They assumed lateral flow to be the cause of snowmelt input which was not covered by the one-dimensional model (Stumpp & Hendry, 2012). Further, non-uniform flow has been found to result from imperfect lateral mixing (Jackisch & Zehe, 2018). Although, as mentioned above, the DMC fluxes are vertically dominated, hence it is unlikely that the lack of lateral flow in our model causes large uncertainties in our simulations. For simulation of isotopic composition, instant mixing was assumed, except for the deeper layer where data were derived from the previous timestep, resulting into better results for deeper soil water isotopic composition, possibly because of longer travel times required for wetting fronts to reach the layer depth of 70 cm. Still, such partial mixing is unlikely to be a major issue for the upper and lower soil compartment, as relatively quick responses in isotopic composition to precipitation events occurred (Landgraf et al., 2022). Interesting for future studies may be to explore the more general value and information content of isotopes in ecohydrological models, for example, how to weight them and how many samples are sufficient to improve simulations adequately (Stevenson et al., 2021). In general, tracer-based models are suitable for testing mixing assumptions as it was shown by several studies (Birkel & Soulsby, 2015; Dehaspe et al., 2018; Mayer-Anhalt et al., 2022; Piovano et al., 2019; Sprenger et al., 2018).

6 | CONCLUSIONS

To better understand ecohydrological processes of the CZ—the dynamic living skin at the Earth's system—we successfully constrained estimates of water fluxes and storages through tracer-aided ecohydrological modelling, which allowed us to follow the fingerprint of precipitation through the soil–plant–atmosphere continuum. We used ecohydrological and stable water isotope data from an intense monitoring programme of a lowland headwater catchment to test a parsimonious, tracer-aided model for its capability to simulate the complex couplings of CZ processes at the plot scale. Further, we aimed to quantify effects of different vegetation covers from a mixed land use catchment (forest, grassland, agroforestry and crops) on water partitioning into blue and green water fluxes.

The model reflected the dynamics of soil moisture (KGE typically > 0.7) and soil water isotopic composition (KGE typically > 0.6) well, although absolute values of simulated soil water isotopes were depleted compared to observed data, probably because of an underestimation of soil evaporation. Water table fluctuation dynamics were also captured well by the simulation of groundwater recharge. The simulated ET was inside ranges of previous studies, whereas simulated recharge was slightly overestimated, although the hydroclimatic conditions of 2021 (snow and summer storm event) may explain the differences to previous studies. Differences between vegetation cover were shown to increase transpiration and interception evaporation in the forest compared to the other sites. *Forest* and *Agroforestry* had increased ET and decreased recharge compared to *Grassland* and *Crops*. Implementing stable water isotopes into the model added confidence in the model results, improved process representation and allowed new insights to be gained into both the systems functioning and model limitations. For future studies, it will be interesting to see how well the model predicts water fluxes and isotopic mixing with more extensive data sets over multiple years (cf. Smith et al., 2021b) and to improve quantitative ecohydrological partitioning estimations under alternative land uses. Overall, the lumped, tracer-aided model with a parsimonious concept showed its potential to capture complex couplings of the CZ through a simple and computationally efficient conceptualisation. Further, the model proved its flexibility and transferability between contrasting vegetation cover and its utility as a tool for applied ecohydrological investigations on flux changes.

AUTHOR CONTRIBUTIONS

Conceptualisation: Dörthe Tetzlaff, Chris Soulsby and Christian Birkel; funding acquisition: Dörthe Tetzlaff and Chris Soulsby; methodology: Dörthe Tetzlaff, Chris Soulsby, Christian Birkel and Jamie Lee Stevenson; investigation: Jessica Landgraf; resources: Dörthe Tetzlaff and Chris Soulsby; software: Christian Birkel, Jamie Lee Stevenson and Jessica Landgraf; supervision: Dörthe Tetzlaff, Chris Soulsby and Christian Birkel; initial draft: Jessica Landgraf; reviewing and editing: Dörthe Tetzlaff, Chris Soulsby, Christian Birkel and Jamie Lee Stevenson.

DATA AVAILABILITY STATEMENT

Research data are not shared.

ORCID

Jessica Landgraf https://orcid.org/0000-0003-3207-7515
Christian Birkel https://orcid.org/0000-0002-6792-852X

REFERENCES

Allen, R.G., Pereira, L.S., Raes, D. & Smith, M. (1998) Crop evapotranspiration-Guidelines for computing crop water requirements-FAO Irrigation and drainage paper 56. *Fao Rome*, 300(9), D05109.

Anabalón, A. & Sharma, A. (2017) On the divergence of potential and actual evapotranspiration trends: an assessment across alternate global datasets. *Earth's Future*, 5(9), 905–917. Available from: https://doi.org/10.1002/2016EF000499

Andréassian, V. (2004) Waters and forests: from historical controversy to scientific debate. *Journal of Hydrology*, 291(1–2), 1–27. Available from: https://doi.org/10.1016/j.jhydrol.2003.12.015

Balist, J., Malekmohammadi, B., Jafari, H.R., Nohegar, A. & Geneletti, D. (2022) Detecting land use and climate impacts on water yield ecosystem service in arid and semi-arid areas. A study in Sirvan River basin-Iran. *Applied Water Science*, 12(1), 4. Available from: https://doi.org/10.1007/s13201-021-01545-8

Birkel, C. & Soulsby, C. (2015) Advancing tracer-aided rainfall–runoff modelling: a review of progress, problems and unrealised potential. *Hydrological Processes*, 29(25), 5227–5240. Available from: https://doi.org/10.1002/hyp.10594

Birkel, C., Soulsby, C. & Tetzlaff, D. (2015) Conceptual modelling to assess how the interplay of hydrological connectivity, catchment storage and tracer dynamics controls nonstationary water age estimates. *Hydrological Processes*, 29(13), 2956–2969. Available from: https://doi.org/10.1002/hyp.10414

Burba, G. (2013) Eddy covariance method for scientific, industrial, agricultural and regulatory applications: a field book on measuring ecosystem gas exchange and areal emission rates. *LI-COR Biosciences*, ISBN 978-0-615-76827-4.

Coenders-Gerrits, A.M.J., Van der Ent, R.J., Bogaard, T.A., Wang-Erlandsson, L., Hrachowitz, M. & Savenije, H.H.G. (2014) Uncertainties in transpiration estimates. *Nature*, 506(7487), E1–E2. Available from: https://doi.org/10.1038/nature12925

Dehaspe, J., Birkel, C., Tetzlaff, D., Sánchez-Murillo, R., Durán-Quesada, A.M. & Soulsby, C. (2018) Spatially distributed tracer-aided modelling to explore water and isotope transport, storage and mixing in a pristine, humid tropical catchment. *Hydrological Processes*, 32(21), 3206–3224. Available from: https://doi.org/10.1002/hyp.13258

Deutscher Wetterdienst. (2022). *DWD [data set]*. Available from: https://opendata.dwd.de/climate_environment/CDC/observations_germany/climate/daily/more_precip/recent/

Douinot, A., Tetzlaff, D., Maneta, M., Kuppel, S., Schulte-Bisping, H. & Soulsby, C. (2019) Ecohydrological modelling with EcH2O-iso to quantify forest and grassland effects on water partitioning and flux ages. *Hydrological Processes*, 33(16), 2174–2191. Available from: https://doi.org/10.1002/hyp.13480

Dubbert, M. & Werner, C. (2019) Water fluxes mediated by vegetation: emerging isotopic insights at the soil and atmosphere interfaces. *New Phytologist*, 221(4), 1754–1763. Available from: https://doi.org/10.1111/nph.15547

Falkenmark, M. & Rockström, J. (2006) The new blue and green water paradigm: breaking new ground for water resources planning and management. *Journal of Water Resources Planning and Management*, 132(3), 129–132. Available from: https://doi.org/10.1061/(ASCE)0733-9496(2006)132:3(129)

Fatichi, S., Pappas, C. & Ivanov, V.Y. (2016) Modeling plant–water interactions: an ecohydrological overview from the cell to the global scale. *Wiley Interdisciplinary Reviews Water*, 3(3), 327–368. Available from: https://doi.org/10.1002/wat2.1125

Foley, J.A., DeFries, R., Asner, G.P., Barford, C., Bonan, G., Carpenter, S.R. et al. (2005) Global consequences of land use. *Science*, 309(5734), 570–574. Available from: https://doi.org/10.1126/science.1111772

Friesen, J. & Van Stan, J.T. (2019) Early European observations of precipitation partitioning by vegetation: a synthesis and evaluation of 19th century findings. *Geosciences*, 9(10), 423. Available from: https://doi.org/10.3390/geosciences9100423

Gelbrecht, J., Fait, M., Dittrich, M. & Steinberg, C. (1998) Use of GC and equilibrium calculations of CO_2 saturation index to indicate whether freshwater bodies in north-eastern Germany are net sources or sinks for atmospheric CO2. *Fresenius' Journal of Analytical Chemistry*, 361(1), 47–53. Available from: https://doi.org/10.1007/s002160050832

Gelbrecht, J., Lengsfeld, H., Pöthig, R. & Opitz, D. (2005) Temporal and spatial variation of phosphorus input, retention and loss in a small catchment of NE Germany. *Journal of Hydrology*, 304(1–4), 151–165. Available from: https://doi.org/10.1016/j.jhydrol.2004.07.028

Geris, J., Tetzlaff, D., McDonnell, J. & Soulsby, C. (2015) The relative role of soil type and tree cover on water storage and transmission in northern headwater catchments. *Hydrological Processes*, 29(7), 1844–1860. Available from: https://doi.org/10.1002/hyp.10289

Gerrits, A.M.J., Pfister, L. & Savenije, H.H.G. (2010) Spatial and temporal variability of canopy and forest floor interception in a beech forest. *Hydrological Processes*, 24(21), 3011–3025. Available from: https://doi.org/10.1002/hyp.7712

Gibson, J.J., Birks, S.J. & Yi, Y. (2016) Stable isotope mass balance of lakes: a contemporary perspective. *Quaternary Science Reviews*, 131, 316–328. Available from: https://doi.org/10.1016/j.quascirev.2015.04.013

Gibson, J.J., Holmes, T., Stadnyk, T.A., Birks, S.J., Eby, P. & Pietroniro, A. (2021) Isotopic constraints on water balance and evapotranspiration partitioning in gauged watersheds across Canada. *Journal of Hydrology: Regional Studies*, 37, 100878. Available from: https://doi.org/10.1016/j.ejrh.2021.100878

Gibson, J.J., Sadek, M.A., Stone, D.J.M., Hughes, C.E., Hankin, S., Cendon, D.I. et al. (2008) Evaporative isotope enrichment as a constraint on reach water balance along a dryland river. *Isotopes in Environmental and Health Studies*, 44(1), 83–98. Available from: https://doi.org/10.1080/10256010801887489

Gonfiantini, R. (1986) Environmental isotopes in lake studies. In: Fritz, P. & Fontes, J.-C. (Eds.) *Handbook of environmental isotope geochemistry*. Amsterdam: Elsevier, pp. 113–168. Available from: https://doi.org/10.1016/B978-0-444-42225-5.50008-5

Grant, G.E. & Dietrich, W.E. (2017) The frontier beneath our feet. *Water Resources Research*, 53(4), 2605–2609. Available from: https://doi.org/10.1002/2017WR020835

Hänsel, S., Hoy, A., Brendel, C. & Maugeri, M. (2022) Record summers in Europe: variations in drought and heavy precipitation during 1901–2018. *International Journal of Climatology*, 42(12), 6235–6257. Available from: https://doi.org/10.1002/joc.7587

Hasselquist, N.J., Benegas, L., Roupsard, O., Malmer, A. & Ilstedt, U. (2018) Canopy cover effects on local soil water dynamics in a tropical agroforestry system: evaporation drives soil water isotopic enrichment. *Hydrological Processes*, 32(8), 994–1004. Available from: https://doi.org/10.1002/hyp.11482

He, Z., Unger-Shayesteh, K., Vorogushyn, S., Weise, S.M., Kalashnikova, O., Gafurov, A. et al. (2019) Constraining hydrological model parameters using water isotopic compositions in a glacierized basin, Central Asia. *Journal of Hydrology*, 571, 332–348. Available from: https://doi.org/10.1016/j.jhydrol.2019.01.048

Horita, J. & Wesolowski, D.J. (1994) Liquid-vapor fractionation of oxygen and hydrogen isotopes of water from the freezing to the critical temperature. *Geochimica et Cosmochimica Acta*, 58(16), 3425–3437. Available from: https://doi.org/10.1016/0016-7037(94)90096-5

Hrachowitz, M., Benettin, P., Van Breukelen, B.M., Fovet, O., Howden, N.J., Ruiz, L. et al. (2016) Transit times—the link between hydrology and water quality at the catchment scale. *Wiley Interdisciplinary Reviews Water*, 3(5), 629–657. Available from: https://doi.org/10.1002/wat2.1155

Jackisch, C. & Zehe, E. (2018) Ecohydrological particle model based on representative domains. *Hydrology and Earth System Sciences*, 22(7), 3639–3662. Available from: https://doi.org/10.5194/hess-22-3639-2018

Jankiewicz, P., Neumann, J., Duijnisveld, W.H.M., Wessolek, G., Wyclsk, P. & Hennings, V. (2005) Abflusshöhe–Sickerwasserrate–Grundwasserneubildung–Drei Themen im Hydrologischen Atlas von Deutschland. *Hydrologie und Wasserbewirtschaftung*, 49, 2–13.

Jasechko, S., Birks, S.J., Gleeson, T., Wada, Y., Fawcett, P.J., Sharp, Z.D. et al. (2014) The pronounced seasonality of global groundwater recharge. *Water Resources Research*, 50(11), 8845–8867. Available from: https://doi.org/10.1002/2014WR015809

Jung, M., Reichstein, M., Ciais, P., Seneviratne, S.I., Sheffield, J., Goulden, M.L. et al. (2019) Recent decline in the global land evapotranspiration trend due to limited moisture supply. *Nature*, 467(7318), 951–954. Available from: https://doi.org/10.1038/nature09396

Kim, J.H. & Jackson, R.B. (2012) A global analysis of groundwater recharge for vegetation, climate, and soils. *Vadose Zone Journal*, 11(1), vzj2011.0021RA. Available from: https://doi.org/10.2136/vzj2011.0021RA

Kleine, L., Tetzlaff, D., Smith, A., Dubbert, M. & Soulsby, C. (2021) Modelling ecohydrological feedbacks in forest and grassland plots under a prolonged drought anomaly in Central Europe 2018–2020. *Hydrological Processes*, 35(8), e14325. Available from: https://doi.org/10.1002/hyp.14325

Kleine, L., Tetzlaff, D., Smith, A., Goldhammer, T. & Soulsby, C. (2021) Using isotopes to understand landscape-scale connectivity in a groundwater-dominated, lowland catchment under drought conditions. *Hydrological Processes*, 35(5), e14197. Available from: https://doi.org/10.1002/hyp.14197

Kleine, L., Tetzlaff, D., Smith, A., Wang, H. & Soulsby, C. (2020) Using water stable isotopes to understand evaporation, moisture stress, and re-wetting in catchment forest and grassland soils of the summer drought of 2018. *Hydrology and Earth System Sciences*, 24(7), 3737–3752. Available from: https://doi.org/10.5194/hess-24-3737-2020

Kling, H., Fuchs, M. & Paulin, M. (2012) Runoff conditions in the upper Danube basin under an ensemble of climate change scenarios. *Journal of Hydrology*, 424, 264–277. Available from: https://doi.org/10.1016/j.jhydrol.2012.01.011

Knighton, J., Saia, S.M., Morris, C.K., Archiblad, J.A. & Walter, M.T. (2017) Ecohydrologic considerations for modeling of stable water isotopes in a small intermittent watershed. *Hydrological Processes*, 31(13), 2438–2452. Available from: https://doi.org/10.1002/hyp.11194

Kool, D., Agam, N., Lazarovitch, N., Heitman, J.L., Sauer, T.J. & Ben-Gal, A. (2014) A review of approaches for evapotranspiration partitioning. *Agricultural and Forest Meteorology*, 184, 56–70. Available from: https://doi.org/10.1016/j.agrformet.2013.09.003

Kottek, M., Grieser, J., Beck, C., Rudolf, B. & Rubel, F. (2006). World map of the Köppen–Geiger climate classification updated. *Meteorologische Zeitschrift*, 15(3), 259–263. Available from: https://doi.org/10.1127/0941-2948/2006/0130

Kuppel, S., Tetzlaff, D., Maneta, M.P. & Soulsby, C. (2018) EcH $_2$ O-iso 1.0: water isotopes and age tracking in a process-based, distributed ecohydrological model. *Geoscientific Model Development*, 11(7), 3045–3069. Available from: https://doi.org/10.5194/gmd-11-3045-2018

Landgraf, J., Tetzlaff, D., Wu, S., Freymüller, J. & Soulsby, C. (2022) Using stable water isotopes to understand ecohydrological partitioning under contrasting land uses in a drought-sensitive rural, lowland catchment. *Hydrological Processes*, 36(12), e14779. Available from: https://doi.org/10.1002/hyp.14779

Liu, J., Wu, H., Cheng, Y., Jin, Z. & Hu, J. (2021) Stable isotope analysis of soil and plant water in a pair of natural grassland and understory of planted forestland on the Chinese loess plateau. *Agricultural Water Management*, 249, 106800. Available from: https://doi.org/10.1016/j.agwat.2021.106800

Lüttger, A., Gerstengarbe, F.-W., Gutsch, M., Hattermann, F., Lasch, P., Murawski, A. et al. (2011) *Klimawandel in der Region Havelland-Fläming*. Potsdam-Institut für Klimafolgenforschung.

Ma, S., Eichelmann, E., Wolf, S., Rey-Sanchez, C. & Baldocchi, D.D. (2020) Transpiration and evaporation in a Californian oak-grass savanna: field measurements and partitioning model results. *Agricultural and Forest Meteorology*, 295, 108204. Available from: https://doi.org/10.1016/j.agrformet.2020.108204

Mayer-Anhalt, L., Birkel, C., Sánchez-Murillo, R. & Schulz, S. (2022) Tracer-aided modelling reveals quick runoff generation and young streamflow ages in a tropical rainforest catchment. *Hydrological Processes*, 36(2), e14508. Available from: https://doi.org/10.1002/hyp.14508

Merlivat, L. (1978) Molecular diffusivities of H ^{2}O ^{16}, HDO ^{16}, and H ^{2}O ^{18} in gases. *The Journal of Chemical Physics*, 69(6), 2864–2871. Available from: https://doi.org/10.1063/1.436884

Moore, G.W. & Heilman, J.L. (2011) Proposed principles governing how vegetation changes affect transpiration. *Ecohydrology*, 4(3), 351–358. Available from: https://doi.org/10.1002/eco.232

Moravec, V., Markonis, Y., Rakovec, O., Svoboda, M., Trnka, M., Kumar, R. et al. (2021) Europe under multi-year droughts: how severe was the 2014–2018 drought period? *Environmental Research Letters*, 16(3), 034062. Available from: https://doi.org/10.1088/1748-9326/abe828

Muñoz Sabater, J. (2019) *ERA5-land hourly data from 1950 to present*. Copernicus Climate Change Service (C3S) Climate Data Store (CDS). Available from: https://doi.org/10.24381/cds.e2161bac [Accessed 25th May 2023].

Neill, A.J., Birkel, C., Maneta, M.P., Tetzlaff, D. & Soulsby, C. (2021) Structural changes to forests during regeneration affect water flux partitioning, water ages and hydrological connectivity: insights from tracer-aided ecohydrological modelling. *Hydrology and Earth System Sciences*, 25(9), 4861–4886. Available from: https://doi.org/10.5194/hess-25-4861-2021

Noordwijk, M.V. (2020) Agroforestry as nexus of sustainable development goals. In: *IOP conference series: earth and environmental science*, Vol. 449, No. 1. IOP Publishing, p. 012001. Available from: https://doi.org/10.1088/1755-1315/449/1/012001

Orlowski, N., Kraft, P., Pferdmenges, J. & Breuer, L. (2016) Exploring water cycle dynamics by sampling multiple stable water isotope pools in a developed landscape in Germany. *Hydrology and Earth System Sciences*, 20(9), 3873–3894. Available from: https://doi.org/10.5194/hess-20-3873-2016

Orth, R. & Destouni, G. (2018) Drought reduces blue-water fluxes more strongly than green-water fluxes in Europe. *Nature Communications*, 9(1), 3602. Available from: https://doi.org/10.1038/s41467-018-06013-7

Owuor, S.O., Butterbach-Bahl, K., Guzha, A.C., Rufino, M.C., Pelster, D.E., Díaz-Pinés, E. et al. (2016) Groundwater recharge rates and surface runoff response to land use and land cover changes in semi-arid environments. *Ecological Processes*, 5(1), 16. Available from: https://doi.org/10.1186/s13717-016-0060-6

Piovano, T.I., Tetzlaff, D., Carey, S.K., Shatilla, N.J., Smith, A. & Soulsby, C. (2019) Spatially distributed tracer-aided runoff modelling and dynamics of storage and water ages in a permafrost-influenced catchment. *Hydrology and Earth System Sciences*, 23(6), 2507–2523. Available from: https://doi.org/10.5194/hess-23-2507-2019

Porporato, A., Feng, X., Manzoni, S., Mau, Y., Parolari, A.J. & Vico, G. (2015) Ecohydrological modeling in agroecosystems: examples and challenges. *Water Resources Research*, 51(7), 5081–5099. Available from: https://doi.org/10.1002/2015WR017289

Qi, W., Ma, C., Xu, H., Zhao, K. & Chen, Z. (2022) A comprehensive analysis method of spatial prioritization for urban flood management based on source tracking. *Ecological Indicators*, 135, 108565. Available from: https://doi.org/10.1016/j.ecolind.2022.108565

Rijal, S. (2019) Agroforestry system: approaches for climate change mitigation and adaptation. *Big Data in Agriculture (BDA)*, 1(2), 23–25. Available from: https://doi.org/10.26480/bda.02.2019.23.25

Roberts, J.M. (2009) The role of forests in the hydrological cycle. *Forests and Forest Plants*, 3, 42–76. ISBN – 978-1-905839-40-7(e-Book Adobe Reader), ISBN-978-1-84826-940-8 (Print (Full Color Edition)).

Rothfuss, Y., Biron, P., Braud, I., Canale, L., Durand, J.L., Gaudet, J.P. et al. (2010) Partitioning evapotranspiration fluxes into soil evaporation and plant transpiration using water stable isotopes under controlled conditions. *Hydrological Processes*, 24(22), 3177–3194. Available from: https://doi.org/10.1002/hyp.7743

Schlesinger, W.H. & Jasechko, S. (2014) Transpiration in the global water cycle. *Agricultural and Forest Meteorology*, 189, 115–117. Available from: https://doi.org/10.1016/j.agrformet.2014.01.011

Shao, R., Zhang, B., Su, T., Long, B., Cheng, L., Xue, Y. et al. (2019) Estimating the increase in regional evaporative water consumption as a result of vegetation restoration over the loess plateau, China. *Journal of Geophysical Research-Atmospheres*, 124(22), 11783–11802. Available from: https://doi.org/10.1029/2019JD031295

Smith, A., Tetzlaff, D., Gelbrecht, J., Kleine, L. & Soulsby, C. (2020) Riparian wetland rehabilitation and beaver re-colonization impacts on hydrological processes and water quality in a lowland agricultural catchment. *Science of the Total Environment*, 699, 134302. Available from: https://doi.org/10.1016/j.scitotenv.2019.134302

Smith, A., Tetzlaff, D., Kleine, L., Maneta, M.P. & Soulsby, C. (2020) Isotope-aided modelling of ecohydrologic fluxes and water ages under mixed land use in Central Europe: the 2018 drought and its recovery. *Hydrological Processes*, 34(16), 3406–3425. Available from: https://doi.org/10.1002/hyp.13838

Smith, A., Tetzlaff, D., Kleine, L., Maneta, M.P. & Soulsby, C. (2021a) Quantifying the effects of land use and model scale on water partitioning and water ages using tracer-aided ecohydrological models. *Hydrology and Earth System Sciences*, 25(4), 2239–2259. Available from: https://doi.org/10.5194/hess-25-2239-2021

Smith, A., Tetzlaff, D., Kleine, L., Maneta, M. & Soulsby, C. (2021b) Upscaling land-use effects on water partitioning and water ages using tracer-aided ecohydrological models. *Hydrology and Earth System Sciences Discussions*, 2020, 1–36.

Smith, A., Tetzlaff, D., Landgraf, J., Dubbert, M. & Soulsby, C. (2022) Modelling temporal variability of in situ soil water and vegetation isotopes reveals ecohydrological couplings in a riparian willow plot. *Biogeosciences*, 19(9), 2465–2485. Available from: https://doi.org/10.5194/bg-19-2465-2022

Soetaert, K. & Petzoldt, T. (2010) Inverse modelling, sensitivity and Monte Carlo analysis in R using package FME. *Journal of Statistical Software*, 33(3), 1–28. Available from: https://doi.org/10.18637/jss.v033.i03

Soulsby, C., Birkel, C. & Tetzlaff, D. (2016) Modelling storage-driven connectivity between landscapes and riverscapes: towards a simple framework for long-term ecohydrological assessment. *Hydrological Processes*, 30(14), 2482–2497. Available from: https://doi.org/10.1002/hyp.10862

Sprenger, M., Leistert, H., Gimbel, K. & Weiler, M. (2016) Illuminating hydrological processes at the soil-vegetation-atmosphere interface with water stable isotopes. *Reviews of Geophysics*, 54(3), 674–704. Available from: https://doi.org/10.1002/2015RG000515

Sprenger, M., Llorens, P., Gallart, F., Benettin, P., Allen, S.T. & Latron, J. (2022) Precipitation fate and transport in a Mediterranean catchment through models calibrated on plant and stream water isotope data. *Hydrology and Earth System Sciences*, 26(15), 4093–4107. Available from: https://doi.org/10.5194/hess-26-4093-2022

Sprenger, M., Tetzlaff, D., Buttle, J., Carey, S.K., McNamara, J.P., Laudon, H. et al. (2018) Storage, mixing, and fluxes of water in the critical zone across northern environments inferred by stable isotopes of soil water. *Hydrological Processes*, 32(12), 1720–1737. Available from: https://doi.org/10.1002/hyp.13135

Stadnyk, T.A. & Holmes, T.L. (2020) On the value of isotope-enabled hydrological model calibration. *Hydrological Sciences Journal*, 65(9), 1525–1538. Available from: https://doi.org/10.1080/02626667.2020.1751847

Stevenson, J.L., Birkel, C., Comte, J.C., Tetzlaff, D., Marx, C., Neill, A. et al. (2023) Quantifying heterogeneity in ecohydrological partitioning in urban green spaces through the integration of empirical and modelling approaches. *Environmental Monitoring and Assessment*, 195(4), 468. Available from: https://doi.org/10.1007/s10661-023-11055-6

Stevenson, J.L., Birkel, C., Neill, A.J., Tetzlaff, D. & Soulsby, C. (2021) Effects of streamflow isotope sampling strategies on the calibration of a tracer-aided rainfall-runoff model. *Hydrological Processes*, 35(6), e14223. Available from: https://doi.org/10.1002/hyp.14223

Stumpp, C. & Hendry, M.J. (2012) Spatial and temporal dynamics of water flow and solute transport in a heterogeneous glacial till: the application of high-resolution profiles of δ18O and δ2H in pore waters. *Journal of Hydrology*, 438, 203–214. Available from: https://doi.org/10.1016/j.jhydrol.2012.03.024

Tague, C.L., Moritz, M. & Hanan, E. (2019) The changing water cycle: the eco-hydrologic impacts of forest density reduction in Mediterranean (seasonally dry) regions. *Wiley Interdisciplinary Reviews Water*, 6(4), e1350. Available from: https://doi.org/10.1002/wat2.1350

Taylor, R.G., Scanlon, B., Döll, P., Rodell, M., Van Beek, R., Wada, Y. et al. (2013) Ground water and climate change. *Nature Climate Change*, 3(4), 322–329. Available from: https://doi.org/10.1038/nclimate1744

Vaché, K.B. & McDonnell, J.J. (2006) A process-based rejectionist framework for evaluating catchment runoff model structure. *Water Resources Research*, 42(2), 1–15. Available from: https://doi.org/10.1029/2005WR004247

Wada, Y., Van Beek, L.P., Van Kempen, C.M., Reckman, J.W., Vasak, S. & Bierkens, M.F. (2010) Global depletion of groundwater resources. *Geophysical Research Letters*, 37(20). Available from: https://doi.org/10.1029/2010GL044571 n/a.

Wang, H., Tetzlaff, D., Dick, J.J. & Soulsby, C. (2017) Assessing the environmental controls on Scots pine transpiration and the implications for water partitioning in a boreal headwater catchment. *Agricultural and Forest Meteorology*, 240, 58–66. Available from: https://doi.org/10.1016/j.agrformet.2017.04.002

Wassenaar, L.I., Hendry, M.J., Chostner, V.L. & Lis, G.P. (2008) High resolution pore water δ2H and δ18O measurements by H$_2$O (liquid)–H$_2$O (vapor) equilibration laser spectroscopy. *Environmental Science & Technology*, 42(24), 9262–9267. Available from: https://doi.org/10.1021/es802065s

Wu, Q., Si, B., He, H. & Wu, P. (2019) Determining regional-scale groundwater recharge with GRACE and GLDAS. *Remote Sensing*, 11(2), 154. Available from: https://doi.org/10.3390/rs11020154

Wu, S., Tetzlaff, D., Yang, X. & Soulsby, C. (2022a) Identifying dominant processes in time and space: time-varying spatial sensitivity analysis for a grid-based nitrate model. *Water Resources Research*, 58(8), e2021WR031149. Available from: https://doi.org/10.1029/2021WR031149

Wu, S., Tetzlaff, D., Yang, X. & Soulsby, C. (2022b) Disentangling the influence of landscape characteristics, hydroclimatic variability and land management on surface water NO$_3$-N dynamics: spatially distributed modeling over 30 yr in a lowland mixed land use catchment. *Water Resources Research*, 58(2), e2021WR030566. Available from: https://doi.org/10.1029/2021WR030566

Wullschleger, S.D., Hanson, P.J. & Todd, D.E. (2001) Transpiration from a multi-species deciduous forest as estimated by xylem sap flow techniques. *Forest Ecology and Management*, 143(1–3), 205–213. Available from: https://doi.org/10.1016/S0378-1127(00)00518-1

Wunsch, A., Liesch, T. & Broda, S. (2022) Deep learning shows declining groundwater levels in Germany until 2100 due to climate change. *Nature Communications*, 13(1), 1221. Available from: https://doi.org/10.1038/s41467-022-28770-2

Zhang, C., Takase, K., Oue, H., Ebisu, N. & Yan, H. (2013) Effects of land use change on hydrological cycle from forest to upland field in a catchment, Japan. *Frontiers of Structural and Civil Engineering*, 7(4), 456–465. Available from: https://doi.org/10.1007/s11709-013-0218-6

Zhou, S., Yu, B., Zhang, Y., Huang, Y. & Wang, G. (2016) Partitioning evapotranspiration based on the concept of underlying water use efficiency. *Water Resources Research*, 52(2), 1160–1175. Available from: https://doi.org/10.1002/2015WR017766

SUPPORTING INFORMATION

Additional supporting information can be found online in the Supporting Information section at the end of this article.